Adv Comput Math (2021) 47: 13
https://doi.org/10.1007/s10444-020-09832-9

A well-balanced high-order scheme on van Leer-type for the shallow water equations with temperature gradient and variable bottom topography

Nguyen Xuan Thanh[1,4] · Mai Duc Thanh[2,4] · Dao Huy Cuong[3]

Received: 18 December 2019 / Accepted: 15 December 2020 /
Published online: 2 February 2021

Abstract

A well-balanced high-order scheme for shallow water equations with variable topography and temperature gradient is constructed. This scheme is of van Leer-type and is based on exact Riemann solvers. The scheme is shown to be able to capture almost exactly the stationary smooth solutions as well as stationary elementary discontinuities. Numerical tests show that the scheme gives a much better accuracy than the Godunov-type scheme and can work well even in the resonant regime. Wave interaction problems are also tested where the scheme possesses a good accuracy. It turns out that the superbee limiter can provide us with more accurate approximations than van Leer's limiter.

Keywords Well-balanced · High-order scheme · Ripa system · Nonconservative · Riemann solver · Van Leer scheme

Mathematics Subject Classification (2010) 35L65 · 65M08 · 76B15

Communicated by: Jan Hesthaven

✉ Mai Duc Thanh
mdthanh@hcmiu.edu.vn

Nguyen Xuan Thanh
mr.nxthanh@gmail.com

Dao Huy Cuong
cuongdh@hcmue.edu.vn

[1] Department of Mathematics and Computer Science, University of Science, 227 Nguyen Van Cu str., District 5, Ho Chi Minh City, Vietnam

[2] Department of Mathematics, International University, Quarter 6, Linh Trung Ward, Thu Duc District, Ho Chi Minh City, Vietnam

[3] Department of Mathematics, Ho Chi Minh City University of Pedagogy, 280 An Duong Vuong str., District 5, Ho Chi Minh City, Vietnam

[4] Vietnam National University, Ho Chi Minh City, Vietnam

1 Introduction

Numerical approximations for fluid flow models involving source terms in nonconservative form have been attractive for many authors in various areas. Often, the nonconservative terms cause lots of inconvenience for standard existing numerical schemes, such as visible oscillations, or the approximations may not be better when the mesh sizes get smaller. In this paper, we aim to construct a well-balanced and high-order numerical scheme of the van Leer type for the following Ripa system:

$$\begin{aligned} &\partial_t h + \partial_x (hu) = 0, \\ &\partial_t (hu) + \partial_x \left(hu^2 + \frac{gh^2\theta}{2} \right) = -gh\theta \partial_x a, \\ &\partial_t (h\theta) + \partial_x (hu\theta) = 0, \end{aligned} \tag{1.1}$$

see [25, 26]. Here, $h = h(x,t)$, $u = u(x,t)$, and $\theta = \theta(x,t)$ denote the water depth, the depth-averaged horizontal velocity, and the potential temperature field, respectively; g is the gravitational constant, and $a = a(x)$ is the bottom topography. Note that the Ripa system (1.1) was used to model ocean currents. It was derived from the Saint-Venant system of shallow water equations, in which the horizontal water temperature fluctuations are taken into account.

In a recent work [33], we proposed a Godunov-type scheme for (1.1), which was shown to have good approximations. The Godunov-type scheme was constructed relying on exact solutions of the local Riemann problem; see [31]. This work develops the method by building a higher order scheme of van Leer's type for (1.1), where the idea of Hancock is used when computing intermediate states instead of using solutions of a generalized Riemann problem (see [16]), for example, for conservation laws (without nonconservative terms). The scheme is built and then tested for all kinds of data in the supercritical region or subcritical region, or both. Especially, the scheme still converges and gives a good accuracy when dealing with the resonant phenomenon. Apart from using solutions of the Riemann problem, we still consider the case of interaction waves for testing the newly constructed van Leer-type scheme. Even in this interesting case of interacting waves, the scheme still converges with a high accuracy. Furthermore, this scheme is shown by numerical tests that it can capture almost exactly the stationary smooth solutions as well as stationary elementary discontinuities.

Numerical schemes for a single conservation law with a nonconservative source term were studied in [3, 5, 6]. Numerical approximations of solutions for shallow water equations with variable topography and nonconservative systems were studied in [7, 14, 15, 17, 19, 22–24, 27]. Godunov-type schemes for multi-phase flow models and other hyperbolic systems of balance laws in nonconservative forms are considered in [2, 21, 29]. High-resolution schemes of van Leer-type were constructed in [9, 10]. Recently, a well-balanced scheme that can capture exactly a new kind of steady-state solutions for the Ripa system was presented in [13]. Such a solution is not an elementary wave, since it is not associated with a characteristic field, and cannot be expressed as a combination of a finite number of elementary waves. However, our scheme in this work will be demonstrated to be able to capture this kind of

steady-state solutions as well. Numerical schemes for the Ripa system were also constructed in [8, 18, 28, 32, 34]. Well-balanced schemes for the model of a fluid flow in a nozzle with variable cross-section were constructed in [20]. Numerical schemes for two-phase flow models were presented in [1, 4, 11, 30]. See also the references therein.

This paper is organized as follows. Basic concepts and terminologies of the system are given in Section 2. The Riemann solver is given in Section 3. Section 4 is devoted to the construction of the van Leer-type scheme for 1.1. Numerical tests are conducted in Section 5. Finally, we address conclusions and discussions in Section 6.

2 Background

2.1 Non-strict hyperbolicity

To investigate basic properties of the system (1.1), one often supplements it with the trivial equation:

$$\partial_t a = 0. \tag{2.1}$$

The system (1.1)–(2.1) can be written under the nonconservative form:

$$\partial_t U + A(U)\partial_x U = 0, \tag{2.2}$$

where

$$U = \begin{pmatrix} h \\ u \\ \theta \\ a \end{pmatrix}, \quad A(U) = \begin{pmatrix} u & h & 0 & 0 \\ g\theta & u & gh/2 & g\theta \\ 0 & 0 & u & 0 \\ 0 & 0 & 0 & 0 \end{pmatrix}.$$

The eigenvalues of the matrix $A(U)$ are given by

$$\lambda_1(U) = u - c, \quad \lambda_2(U) = u, \quad \lambda_3(U) := u + c, \quad \lambda_4(U) := 0, \tag{2.3}$$

and the corresponding eigenvectors can be chosen as

$$r_1(U) = \begin{pmatrix} h \\ -c \\ 0 \\ 0 \end{pmatrix}, \quad r_2(U) = \begin{pmatrix} h \\ 0 \\ -2\theta \\ 0 \end{pmatrix}, \quad r_3(U) = \begin{pmatrix} h \\ c \\ 0 \\ 0 \end{pmatrix}, \quad r_4(U) = \begin{pmatrix} c^2 \\ -gu\theta \\ 0 \\ u^2 - c^2 \end{pmatrix}, \tag{2.4}$$

where

$$c = \sqrt{gh\theta}.$$

Let us define the strictly hyperbolic regions:

$$\begin{aligned} G_1 &= \Big\{U : \lambda_4(U) < \lambda_1(U)\Big\}, \\ G_2 &= \Big\{U : \lambda_1(U) < \lambda_4(U) < \lambda_2(U)\Big\}, \\ G_3 &= \Big\{U : \lambda_2(U) < \lambda_4(U) < \lambda_3(U)\Big\}, \\ G_4 &= \Big\{U : \lambda_3(U) < \lambda_4(U)\Big\}. \end{aligned} \tag{2.5}$$

The characteristic fields $(\lambda_i, r_i), i = 1, 2, 3, 4$, may coincide on certain surfaces. More precisely,

$$\mathcal{C}^+ = \Big\{U : \lambda_1(U) = \lambda_4(U)\Big\},$$
$$\mathcal{C}^0 = \Big\{U : \lambda_2(U) = \lambda_4(U)\Big\},$$
$$\mathcal{C}^- = \Big\{U : \lambda_3(U) = \lambda_4(U)\Big\}.$$

In addition, it is clear that the first and third characteristic fields (λ_1, r_1), (λ_3, r_3) are *genuinely nonlinear*, since

$$-\nabla\lambda_1 \cdot r_1 = \nabla\lambda_3 \cdot r_3 = \frac{3c}{2},$$

and that the second and fourth characteristic fields (λ_2, r_2), (λ_4, r_4) are *linearly degenerate*, since

$$\nabla\lambda_2 \cdot r_2 = \nabla\lambda_2 \cdot r_4 = 0.$$

The *generalized Froude number* is defined by

$$Fr(U) = \frac{|u|}{c}.$$

If $Fr(U) > 1$, then U is called a *supercritical state*; if $Fr(U) < 1$, then U is called a *subcritical state*; if $Fr(U) = 1$, then U is called a *critical state*.

2.2 Rarefaction waves

We will consider rarefaction waves of the system (1.1)–(2.1), which are piecewise smooth self-similar solutions of the form:

$$U(x, t) = V(\xi), \quad \xi = \frac{x}{t}, \quad x \in \mathbb{R}, t > 0.$$

Substituting this into (2.2), we can see that rarefaction waves are solutions of the following initial-value problem for ordinary differential equations:

$$\begin{aligned} &\frac{dV(\xi)}{d\xi} = r_j(V(\xi)), \quad \xi \geq \lambda_j(U_0), \\ &V(\lambda_j(U_0)) = U_0, \quad j = 1, 3, \end{aligned} \tag{2.6}$$

where the eigenvectors r_1 and r_3 are given (2.4). In particular, it holds along the integral curves that

$$\frac{d\theta(\xi)}{d\xi} = \frac{da(\xi)}{d\xi} = 0,$$

which means that the temperature θ and the bottom topography a remain constant through any rarefaction fan; see [31]. Then, we have the two following results:

Firstly, the forward curve of 1-rarefaction waves $\mathcal{R}_1(U_0)$ starting from a given left-hand state U_0, which consists of all the right-hand states U that can be connected to U_0 by a rarefaction wave associated with the first characteristic field:

$$\begin{aligned} \mathcal{R}_1(U_0): \quad & a = a_0, \quad \theta = \theta_0, \\ & u = u_0 - 2\sqrt{g\theta_0}(\sqrt{h} - \sqrt{h_0}), \quad h < h_0. \end{aligned} \tag{2.7}$$

Secondly, the backward curve of 3-rarefaction waves $\mathcal{R}_3^B(U_0)$ starting from a given right-hand state U_0, which consists of all the left-hand states U that can be connected to U_0 by a rarefaction wave associated with the third characteristic field:

$$\begin{aligned} \mathcal{R}_3^B(U_0): \quad & a = a_0, \quad \theta = \theta_0, \\ & u = u_0 + 2\sqrt{g\theta_0}(\sqrt{h} - \sqrt{h_0}), \quad h < h_0. \end{aligned} \tag{2.8}$$

2.3 Shock waves

A *shock wave* of (1.1)–(2.1) is a weak solution of the form:

$$U(x,t) = \begin{cases} U_-, & x < \sigma t, \\ U_+, & x > \sigma t, \end{cases} \tag{2.9}$$

where $\sigma = \sigma(U_-, U_+)$ is the speed of the shock wave; U_-, U_+ are the left-hand and right-hand states, respectively.

With the Rankine-Hugoniot relation associated with (2.1), we have:

$$-\sigma[a] = 0, \tag{2.10}$$

where $[a] = a_+ - a_-$ is the jump of the quantity a across the shock wave. Let us fix a left-hand state $U_- = U_0 = (h_0, u_0, \theta_0, a_0)$, and look for all right-hand states $U = U_+$ of the shock (2.9). Equation (2.10) implies that there are two possibilities across a shock wave:

(i) Either the bottom topography a remains constant,
(ii) Or the speed $\sigma = 0 = \lambda_4(U_\pm)$.

In the second case (ii), the contact discontinuity is *stationary* since it travels with zero speed.

In case (i), the bottom topography a remains constant. Consequently, the system (1.1)–(2.1) can be reduced to the following shallow water equations in conservative form:

$$\begin{aligned} &\partial_t h + \partial_x(hu) = 0, \\ &\partial_t(hu) + \partial_x\Big(hu^2 + \frac{gh^2\theta}{2}\Big) = 0, \\ &\partial_t(h\theta) + \partial_x(hu\theta) = 0. \end{aligned} \tag{2.11}$$

The associated Rankine-Hugoniot relations for (2.11) are given by

$$\begin{aligned} &-\sigma[h] + [hu] = 0, \\ &-\sigma[hu] + \Big[hu^2 + \frac{gh^2\theta}{2}\Big] = 0, \\ &-\sigma[h\theta] + [hu\theta] = 0. \end{aligned} \tag{2.12}$$

Transforming the relations (2.12), we obtain:

$$\begin{aligned} &h_+(u_+ - \sigma) = h_-(u_- - \sigma) =: M, \\ &M(u_+ - u_-) + \frac{g}{2}\Big(h_+^2\theta_+ - h_-^2\theta_-\Big) = 0, \\ &M(\theta_+ - \theta_-) = 0. \end{aligned} \tag{2.13}$$

In the case $M \neq 0$, the relations (2.13) are equivalently written:

$$\begin{aligned} &M = \frac{u_+ - u_-}{\frac{1}{h_+} - \frac{1}{h_-}}, \\ &(u_+ - u_-)^2 = \frac{g\theta_-}{2}(h_+ - h_-)^2\Big(\frac{1}{h_+} + \frac{1}{h_-}\Big), \\ &\theta_+ = \theta_-. \end{aligned} \tag{2.14}$$

A shock wave (2.9) associated with the nonlinear characteristic fields $(\lambda_i, r_i), i = 1, 3$ is required to fulfil the Lax shock inequalities

$$\lambda_i(U_+) < \sigma(U_-, U_+) < \lambda_i(U_-), \quad i = 1, 3, \tag{2.15}$$

as the admissibility criterion.

- For 1-Lax shock (discontinuity wave associated with the first characteristic field), (2.14) and (2.15) imply that

$$M > 0, \quad h_+ > h_-, \quad u_+ < u_-. \tag{2.16}$$

- For 3-Lax shock (discontinuity wave associated with the third characteristic field), (2.14) and (2.15) imply that

$$M < 0, \quad h_- > h_+, \quad u_- > u_+. \tag{2.17}$$

The set of all right-hand states that can be connected to a given left-hand state U_0 by 1-Lax shock forms a curve, denoted by $\mathcal{S}_1(U_0)$

$$\begin{aligned} \mathcal{S}_1(U_0): \quad &a = a_0, \quad \theta = \theta_0, \\ &u = u_0 - \sqrt{\frac{g\theta_0}{2}}(h - h_0)\sqrt{\frac{1}{h} + \frac{1}{h_0}}, \quad h > h_0. \end{aligned} \tag{2.18}$$

Similarly, the set of all left-hand states that can be connected to a given right-hand state U_0 by 3-Lax shock forms a curve, denoted by $\mathcal{S}_3^B(U_0)$

$$\begin{aligned} \mathcal{S}_3^B(U_0): \quad &a = a_0, \quad \theta = \theta_0, \\ &u = u_0 + \sqrt{\frac{g\theta_0}{2}}(h - h_0)\sqrt{\frac{1}{h} + \frac{1}{h_0}}, \quad h > h_0, \end{aligned} \tag{2.19}$$

see [31].

The shock speeds in the nonlinear characteristic fields may coincide with the characteristic speed of the linearly degenerate field as stated in the following lemma.

Lemma 2.1 (Lem. 2.1, [21]) *Consider the projection onto the (h,u)-plane. To every $U_L=(h_L,u_L)\in G_1$, there exists exactly one point $U^{\#}\in\mathcal{S}_1(U_L)\cap G_2$ such that the $1-$shock speed $\sigma_1(U_L,U^{\#})=0$. The state $U^{\#}=(h^{\#},u^{\#})$ is defined by*

$$h^{\#}=\frac{-h_L+\sqrt{h_L^2+8h_Lu_L^2/g\theta_L}}{2},\quad u^{\#}=\frac{u_Lh_L}{h^{\#}}.$$

Moreover, for any $U\in\mathcal{S}_1(U_L)$, the shock speed $\sigma_1(U_L,U)>0$ if and only if U is located above $U^{\#}$ on $\mathcal{S}_1(U_L)$.

From the above results, the wave curves in nonlinear characteristic fields can be defined by

$$\begin{aligned}&\mathcal{W}_1(U_0)=\mathcal{S}_1(U_0)\cup\mathcal{R}_1(U_0),\\&\mathcal{W}_3^B(U_0)=\mathcal{S}_3^B(U_0)\cup\mathcal{R}_3^B(U_0).\end{aligned}\tag{2.20}$$

From (2.20), we can write in detail that the curves $\mathcal{W}_1(U_0),\mathcal{W}_3^B(U_0)$ can be parameterized as

$$\begin{aligned}\mathcal{W}_1(U_0):u=\omega_1(U_0,h)&=\begin{cases}u_0-\sqrt{\frac{g\theta_0}{2}}(h-h_0)\sqrt{\frac{1}{h}+\frac{1}{h_0}}, & h>h_0,\\ u_0-2\sqrt{g\theta_0}(\sqrt{h}-\sqrt{h_0}), & h<h_0,\end{cases}\\ \mathcal{W}_3^B(U_0):u=\omega_3^B(U_0,h)&=\begin{cases}u_0+\sqrt{\frac{g\theta_0}{2}}(h-h_0)\sqrt{\frac{1}{h}+\frac{1}{h_0}}, & h>h_0,\\ u_0+2\sqrt{g\theta_0}(\sqrt{h}-\sqrt{h_0}), & h<h_0.\end{cases}\end{aligned}\tag{2.21}$$

In the case $M=0$, the relations (2.13) become

$$\begin{aligned}&\sigma=u_+=u_-,\\&h_+^2\theta_+=h_-^2\theta_-.\end{aligned}\tag{2.22}$$

Since $\sigma=u_\pm=\lambda_2(U_\pm)$, the discontinuity wave corresponding to this case is called the 2-contact wave. The curve of 2-contact discontinuities can be parameterized by h which starts from a given state U_0 as follows:

$$\begin{aligned}\mathcal{W}_2(U_0):\quad &a=a_0,\quad u=u_0,\\ &\theta=\frac{h_0^2\theta_0}{h^2},\quad h>0.\end{aligned}\tag{2.23}$$

A 2-contact discontinuity may be referred to as a *material contact*; see [31].

2.4 Stationary contact discontinuities

It is easy to see that stationary smooth solutions of (1.1) satisfy

$$\begin{aligned}&(hu)'=0,\\&\left(hu^2+\frac{g}{2}h^2\theta\right)'+gh\theta a'=0,\\&(hu\theta)'=0,\end{aligned}\tag{2.24}$$

where $(.)' = d(.)/dx$.

Theorem 2.2 (Theorem 2.2, [33]) *(a) Any solution of the following system of ordinary differential equations:*

$$\begin{aligned} &(hu)' = 0, \\ &\left(\frac{u^2}{2} + g\theta(h+a)\right)' = 0, \\ &\theta' = 0, \end{aligned} \tag{2.25}$$

is a stationary smooth solution of (1.1).

(b) Any discontinuity (2.9) *with speed* $\sigma = 0$ *satisfying the jump relations*

$$\begin{aligned} &[hu] = 0, \\ &\left[\frac{u^2}{2} + g\theta(h+a)\right] = 0, \\ &[\theta] = 0, \end{aligned} \tag{2.26}$$

is a weak solution of (1.1) *in the sense of nonconservative product corresponding to the path* $s \in [0,1] \mapsto \kappa(s) := \Big(h(s), u(s), \theta(s), a(s)\Big)$ *defined by* (2.25) *such that* $\kappa(0) = (h_-, u_-, \theta_-, a_-)$ *and* $\kappa(1) = (h_+, u_+, \theta_+, a_+)$*; see* [12].

(c) The integral curve associated with the characteristic field (λ_4, r_4) *is a solution of* (2.25).

Therefore, a 4-contact discontinuity of (1.1) is the one satisfying (2.26). Since 4-contact discontinuities travel with zero speed, they are referred to as stationary contact discontinuities.

It is interesting to remark in the following on one kind of stationary waves of (1.1); see [13]. Observe that from the third equation of (2.24), one may obtain

$$(hu)'\theta + (hu)\theta' = 0.$$

Using the first equation in (2.24), the last equation becomes

$$u\theta' = 0$$

which means that either $\theta' = 0$ or $u = 0$. In the first case, we obtain the 4-contact discontinuities as argued above. In the second case, where $u = 0$, one may get from the second equation of (2.24):

$$2\theta(h+a)' + h\theta' = 0.$$

And so, if one assumes that $h' = 0$, then the last equation yields

$$(2a + h\ln\theta)' = 0$$

which leads to a family of stationary solutions of the form

$$u = 0, \quad [h] = 0, [2a + h\ln\theta] = 0.$$

It is easy to see that this curve is tangent to the vector field

$$s(U) = (0, 0, 1, -h/(2\theta))^T$$

which is not parallel to any of the eigenvectors $r_i(U_0)$ at U_0, $i = 1, 2, 3, 4$. Therefore, discontinuities given by this family are not elementary waves. Since solutions of the Riemann problem consist of a finite number of elementary waves, these stationary discontinuities are not involved in the construction of solutions of the Riemann problem.

2.5 Admissible stationary contact discontinuities

It is not the case that all stationary contact discontinuities are admissible. We will discuss about this in the following.

Given a state U_0 and bottom levels on both sides of the stationary contact $a \neq a_0$, the water height h can be resolved when other known quantities from the second equation of (2.26). From this equation, we can obtain a function depending on h as follows:

$$\varphi(h) = 2g\theta_0 h^3 + (2g\theta_0(a - a_0 - h_0) - u_0^2)h^2 + h_0^2 u_0^2 = 0. \tag{2.27}$$

We have the following result:

$$a \leq a_{\max}(U_0) := a_0 + \frac{1}{2g\theta_0}\left((g\theta_0 h_0)^{1/3} - u_0^{2/3}\right)^2 (2(g\theta_0 h_0)^{1/3} + u_0^{2/3}), \tag{2.28}$$

see [31].

The formula (2.28) means that $a_{\max}(U_0) \geq a_0$ and the equality holds only if U_0 belongs to the non-strictly hyperbolic surfaces. Note that if the inequality in (2.28) is strict, i.e., $a < a_{\max}(U_0)$, then the two roots are distinct: $h_1(a) < h_* < h_2(a)$ where

$$h_* = \frac{u_0^2 + 2g\theta_0(a_0 + h_0 - a)}{3g\theta_0}.$$

As a result, whenever (2.28) holds, there are two states $U_+ = U_i$ so that a stationary contact discontinuity from $U_- = U_0$ is possible. The locations of these states can be determined in the following lemma:

Lemma 2.3 (Lemma 3.1, [31]) *Assume that $a < a_{\max}(U_0)$, where $a_{\max}(U_0)$ is defined by (2.28). The function φ defined by (2.27) admits two distinct roots $h_1 < h_2$. Moreover, the state U_1 using the smaller root h_1 belongs to G_1 if $u_0 > 0$ and belongs to G_4 if $u_0 < 0$; the state U_2 using the larger root h_2 lies in G_2 if $u_0 > 0$ and lies in G_3 if $u_0 < 0$.*

To select a unique Riemann solution, the following admissibility criterion for stationary contact discontinuities is imposed; see [31]:

(MC) Along any stationary curve $\mathcal{W}_4(U_0)$, the bottom level a is monotone as a function of h. The total variation of the bottom-level component of any Riemann solution must not exceed $|a_L - a_R|$, where a_L, a_R are left-hand and right-hand bottom levels.

Lemma 2.4 (Lemma 3.2, [31]) *Assume that* $a < a_{\max}(U_0)$*, where* $a_{\max}(U_0)$ *is defined by* (2.28)*. The monotonicity criterion selects the following admissible stationary contact wave.*

i *If* $U_0 \in G_1 \cup G_4$*, then only the stationary contact using the smaller root* h_1 *of* φ *defined by* (2.27) *is selected.*

ii *If* $U_0 \in G_2 \cup G_3$*, then only the stationary contact using the larger root* h_2 *of* φ *defined by* (2.27) *is selected.*

Elementary waves of (1.1), which make up solutions of the Riemann problem, are defined in the following.

Definition 2.5 Elementary waves for the system (1.1) and (2.1) are the following ones: Lax shocks, rarefaction waves, material contact discontinuities, and admissible stationary contact discontinuities.

3 The exact Riemann solver

Exact solutions of the Riemann problem for the Ripa system (1.1) have been presented in [31]. In this section, we will briefly recall these solutions for a reader to easily follow the construction of the van Leer-type scheme in the next section. As usual, the solutions of the Riemann problem are combined by a finite number of elementary waves including shock waves, rarefaction waves, contact waves, and stationary waves. It is sufficient to consider only the Riemann data in $G_1 \cup C_+ \cup G_2$ because the other cases can similarly be obtained. The constructions will be based on the left-hand state U_L.

Notations The following notations will be used in this section to construct the Riemann solutions:

(i) $\mathcal{W}_i(U_1, U_2)$: an i-wave connecting a state U_1 and a state U_2, where $\mathcal{W} = S$: Lax shock, $\mathcal{W} = R$: rarefaction wave, $i = 1, 2, 3, 4$;

(ii) $\mathcal{W}_i(U_1, U_2) \rightarrow \mathcal{W}_j(U_2, U_3)$: an i-wave from the left-hand state U_1 to the right-hand state U_2 is followed by a j-wave from the left-hand state U_2 to the right-hand state u_3;

(iii) $\mathcal{W}_i(U_1, U_2) \leftarrow \mathcal{W}_j(U_2, U_3)$: an i-wave from the right-hand state U_1 to the left-hand state U_2 is preceded by a j-wave from the right-hand state U_2 to the left-hand state U_3;

(iv) The (forward) curve $\mathcal{W}_{i\rightarrow j}(U_0)$ consists of all right-hand states U which can be reached from U_0 using an i-wave from the left-hand state U_0 to some intermediate right-hand state $U_1 \in \mathcal{W}_i(U_0)$, followed by a j-wave from the left-hand state U_1 to the right-hand state U;

(v) The (backward) curve $\mathcal{W}_{i\leftarrow j}(U_0)$ consists of all left-hand states U which can be reached from U_0 using an i-wave from the right-hand state U_0 to some intermediate left-hand state $U_1 \in \mathcal{W}_i(U_0)$, preceded by a j-wave from the right-hand state U_1 to the left-hand state U;

(vi) U^s, U^b denote the states resulted by stationary contact discontinuity wave from U;
(vii) $U^{\#}$ denotes the state resulting from a zero-speed shock wave from U;
(viii) $U^{\pm} = \mathcal{W}_1(U_L) \cap \mathcal{C}^{\pm}$;
(ix) $U^0 = \mathcal{W}_1(U_L) \cap \mathcal{C}^0$.

3.1 Case A: $U_L \in G_1 \cup \mathcal{C}^+$

In this subsection, three constructions A1, A2, and A3 will be built in the case of U_L starting from G_1.

Construction A1 The left-hand and right-hand states are both supercritical.

The solution starts from a stationary wave from U_L to the state U_1, then followed by a wave curve $\mathcal{W}_1$ from U_1 to the state U_2, then followed by a 2-contact discontinuity from U_2 to the state U_3, then followed by a wave curve $\mathcal{W}_3$ from U_3 to the state U_R.

As a result, the Riemann solution for the system (1.1) is in the form of

$$\mathcal{W}_4(U_L, U_1) \to \mathcal{W}_1(U_1, U_2) \to \mathcal{W}_2(U_2, U_3) \to \mathcal{W}_3(U_3, U_R). \tag{3.1}$$

See Fig. 1.

Construction A2 Supercritical left-hand state and subcritical right-hand state.

The solution starts from a 1-shock wave from U_L to a state U_1, then followed by a stationary wave from U_1 to U_2, then followed by a 2-contact discontinuity from U_2 to the state U_3, then followed by a curve wave $\mathcal{W}_3$ from U_3 to U_R.

As a result, the Riemann solution for the system (1.1) is in the form of

$$\mathcal{W}_1(U_L, U_1) \to \mathcal{W}_4(U_1, U_2) \to \mathcal{W}_2(U_2, U_3) \to \mathcal{W}_3(U_3, U_R). \tag{3.2}$$

See Fig. 2.

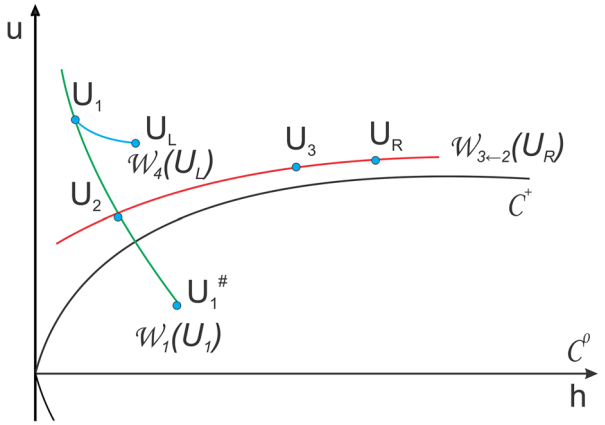

Fig. 1 A Riemann solution of the form (3.1) in Construction A1

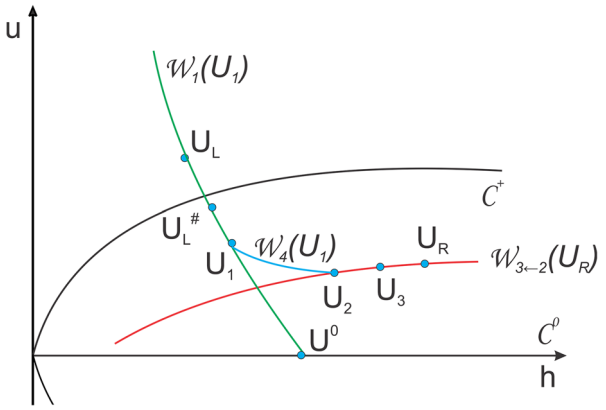

Fig. 2 A Riemann solution of the form (3.2) in Construction A2

Construction A3 Supercritical left-hand state and right-hand state near the critical curve: colliding waves.

The solution starts from a stationary wave from U_L to U_1,

then followed by a zero-speed 1-shock wave from U_1 to U_2, then followed by a stationary wave from U_2 to U_3, then followed by a 2-contact discontinuity from U_3 to the state U_4, then followed by a curve wave $\mathcal{W}_3$ from U_4 to U_R.

As a result, the Riemann solution for the system (1.1) is in the form of

$$\mathcal{W}_4(U_L, U_1) \to \mathcal{W}_1(U_1, U_2) \to \mathcal{W}_4(U_2, U_3) \to \mathcal{W}_2(U_3, U_4) \to \mathcal{W}_3(U_4, U_R). \tag{3.3}$$

See Fig. 3.

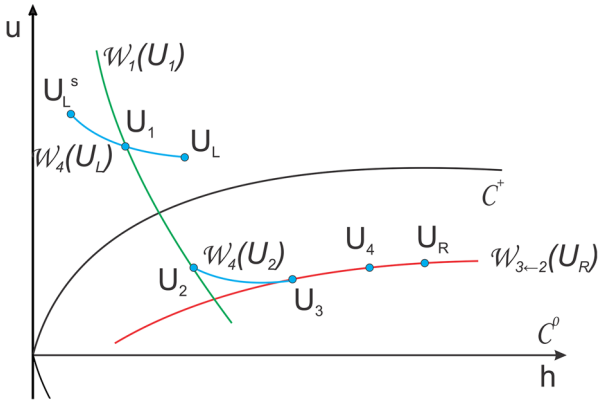

Fig. 3 A Riemann solution of the form (3.3) in Construction A3

3.2 Case B: $U_L \in G_2$

In this subsection, three constructions B1, B2, and B3 will be built in the case of U_L starting from G_2.

Construction B1 Subcritical left-hand state and supercritical right-hand state.

The solution starts from a 1-rarefaction wave from U_L to U_1, then followed by a stationary wave from U_1 to U_2, then followed by a curve wave $\mathcal{W}_1$ from U_2 to U_3, then followed by a 2-contact discontinuity from U_3 to the state U_4, then followed by a curve wave $\mathcal{W}_3$ from U_4 to U_R.

As a result, the Riemann solution for the system (1.1) is in the form of

$$\mathcal{W}_1(U_L, U_1) \to \mathcal{W}_4(U_1, U_2) \to \mathcal{W}_1(U_2, U_3) \to \mathcal{W}_2(U_3, U_4) \to \mathcal{W}_3(U_4, U_R). \tag{3.4}$$

See Fig. 4.

Construction B2 The left-hand and right-hand states are both subcritical.

The solution starts from a curve wave $\mathcal{W}_1$ from U_L to U_1, then followed by a stationary wave from U_1 to U_2, then followed by a 2-contact discontinuity from U_2 to the state U_3, then followed by a curve wave $\mathcal{W}_3$ from U_3 to U_R.

As a result, the Riemann solution for the system (1.1) is in the form of

$$\mathcal{W}_1(U_L, U_1) \to \mathcal{W}_4(U_1, U_2) \to \mathcal{W}_2(U_2, U_3) \to \mathcal{W}_3(U_3, U_R). \tag{3.5}$$

See Fig. 5.

Construction B3 Subcritical left-hand state and right-hand state near the critical curve: colliding waves.

The solution starts from a 1-rarefaction wave from U_L to U_1, then followed by a stationary wave from U_1 to U_2, then followed by a zero-speed 1-shock wave

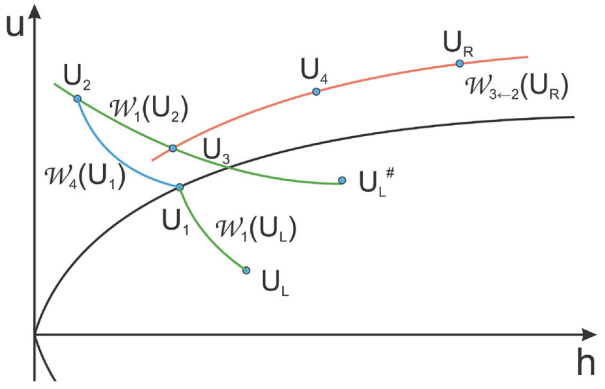

Fig. 4 A Riemann solution of the form (3.4) in Construction B1

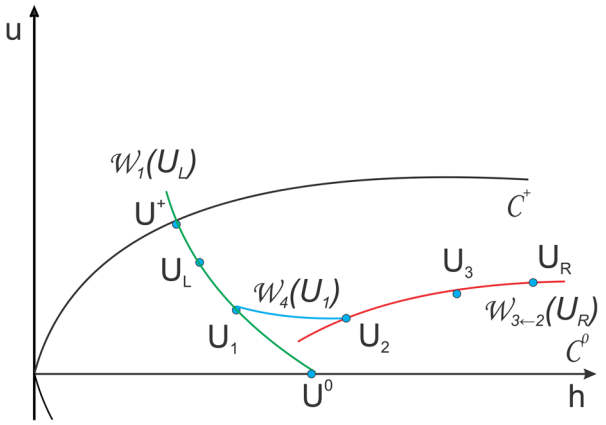

Fig. 5 A Riemann solution of the form (3.5) in Construction B2

from U_2 to U_3, then followed by a stationary wave from U_3 to U_4, then followed by a 2-contact discontinuity from U_4 to the state U_5, then followed by a curve wave $\mathcal{W}_3$ from U_5 to U_R. Observe that h_2 is smaller root of $\varphi(U_1, a_2) = 0$ and h_3^b is bigger root of $\varphi(U_3, a_R) = 0$ by using Newton's method.

As a result, the Riemann solution for the system (1.1) is in the form of

$$\mathcal{W}_1(U_L, U_1) \to \mathcal{W}_4(U_1, U_2) \to \mathcal{W}_1(U_2, U_3) \to \mathcal{W}_4(U_3, U_4) \to \mathcal{W}_2(U_4, U_5) \to \mathcal{W}_3(U_5, U_R). \tag{3.6}$$

See Fig. 6.

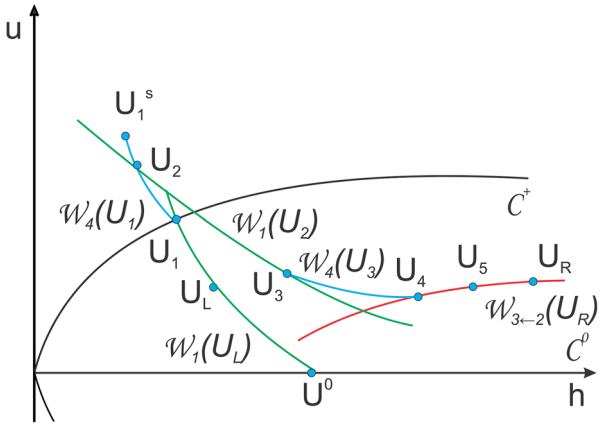

Fig. 6 A Riemann solution of the form (3.6) in Construction B3

4 Building a van Leer-type scheme

In this section, we will build up a van Leer-type scheme for the system (1.1) relying on the constructions of Riemann solutions in the previous section. Let us set

$$U = \begin{pmatrix} h \\ hu \\ h\theta \\ a \end{pmatrix}, \quad F(U) = \begin{pmatrix} hu \\ hu^2 + \dfrac{gh^2\theta}{2} \\ hu\theta \\ 0 \end{pmatrix}, \quad H(U) = \begin{pmatrix} 0 \\ -gh\theta \\ 0 \\ 0 \end{pmatrix}. \tag{4.1}$$

We can re-write the system (1.1)–(2.1) in the form

$$\partial_t U + \partial_x F(U) = H(U)\partial_x a. \tag{4.2}$$

The problem has the initial condition as follows:

$$U(x,0) = U_0(x), \quad x \in \mathbb{R}, \tag{4.3}$$

then, the discrete initial values $U^0 = (U_j^0)_{j\in\mathbb{Z}}$ are given by the average value

$$U_j^0 = \frac{1}{\Delta x}\int_{x_{j-1/2}}^{x_{j+1/2}} U_0(x)dx, \quad j \in \mathbb{Z}. \tag{4.4}$$

4.1 Godunov-type scheme

In this subsection, let us recall Godunov-type scheme in [33]. Suppose that $U^n = (U_j^n)_{j\in\mathbb{Z}}$ is known. We define the approximation $U^{n+1} = (U_j^{n+1})_{j\in\mathbb{Z}}$ of $U(.,t_{n+1})$ as follows:

(i) We extend the sequence U^n as a piecewise constant function $U_{p.con}(.,t_n)$ defined by

$$U_{p.con}(x,t_n) = U_j^n, \quad x_{j-1/2} < x < x_{j+1/2}, \quad j \in \mathbb{Z}. \tag{4.5}$$

(ii) We solve the local Riemann problems for (4.2) with the initial condition

$$U(x,0) = U_{p.con}(x,t_n), \tag{4.6}$$

to find the solution $U(.,\Delta t)$. This solution is obtained by solving a juxtaposition of local Riemann problems, so

$$U(x,t) = U_{exact}\Big(\frac{x - x_{j+1/2}}{t}; U_j^n, U_{j+1}^n\Big), \quad x_j < x < x_{j+1}, \quad j \in \mathbb{Z}, \tag{4.7}$$

where $U_{exact}\Big(\dfrac{x}{t}; U_L, U_R\Big)$ denote the exact solution of the Riemann problem for (4.2) corresponding to the Riemann data (U_L, U_R).

(iii) We project ($\mathbb{L}^2$-projection) the exact solution $U(.,\Delta t)$ onto the piecewise constant functions, i.e.,

$$U_j^{n+1} = \frac{1}{\Delta x}\int_{x_{j-1/2}}^{x_{j+1/2}} U(x,\Delta t)dx. \tag{4.8}$$

Provided we assume the C.F.L. condition:

$$\frac{\Delta t}{\Delta x}\max\{|\lambda_k(U_j^n)| : k = 1, 2, 3, 4\} \le \frac{1}{2}, \tag{4.9}$$

so that the waves issued from the points $x_{j-1/2}$ and $x_{j+1/2}$ do not interact. Since the a-component is constant in each interval $(x_{j-1/2}, x_{j+1/2})$, then the right-hand side of (4.2) vanishes. The Godunov-type scheme is defined by

$$U_j^{n+1} = U_j^n - \frac{\Delta t}{\Delta x}\Big(F(U_{exact}(0-; U_j^n, U_{j+1}^n)) - F(U_{exact}(0+; U_{j-1}^n, U_j^n))\Big), \tag{4.10}$$

where $U_{exact}(0-; U_j^n, U_{j+1}^n)$, $U_{exact}(0+; U_{j-1}^n, U_j^n)$ are determined as in [33].

4.2 van Leer-type scheme

Suppose $U^n = (U_j^n)_{j\in\mathbb{Z}}$ is known. We define the approximation $U^{n+1} = (U_j^{n+1})_{j\in\mathbb{Z}}$ of $U(., t_{n+1})$ as follows:

(i) We extend the sequence U^n as a piecewise linear function $U_{p.lin}(., t_n)$ defined by

$$U_{p.lin}(x, t_n) = U_j^n + \frac{S_j^n}{\Delta x}(x - x_j), \quad x_{j-1/2} < x < x_{j+1/2}, \quad j \in \mathbb{Z}, \tag{4.11}$$

where slopes $S_j^n = (s_{j,1}^n, s_{j,2}^n, s_{j,3}^n, s_{j,4}^n)$ are defined as follows:

$$S_j^n = (U_{j+1}^n - U_j^n)\Theta(\rho_j^n),$$
$$\rho_j^n = \frac{U_j^n - U_{j-1}^n}{U_{j+1}^n - U_j^n},$$

We can use any limiter function in two following one:

$$\begin{bmatrix} \Theta(\rho) = \max(0, \min(1, 2\rho), \min(\rho, 2)), & \text{the superbee limiter,} \\ \Theta(\rho) = \dfrac{|\rho| + \rho}{1 + |\rho|}, & \text{van Leer's limiter.} \end{bmatrix} \tag{4.12}$$

(ii) We solve the local Riemann problems for (4.2) with the initial condition

$$U(x, 0) = U_{p.lin}(x, t_n), \tag{4.13}$$

to find the solution $U(., \Delta t)$.

(iii) We project ($\mathbb{L}^2$-projection) the exact solution $U(., \Delta t)$ onto the piecewise constant functions, i.e.,

$$U_j^{n+1} = \frac{1}{\Delta x}\int_{x_{j-1/2}}^{x_{j+1/2}} U(x, \Delta t)dx. \tag{4.14}$$

Provided we assume the C.F.L. condition:

$$\frac{\Delta t}{\Delta x}\max\{|\lambda_k(U_j^n)| : k = 1, 2, 3, 4\} \le \frac{1}{2}, \tag{4.15}$$

so that the waves issued from the points $x_{j-1/2}$ and $x_{j+1/2}$ do not interact.

In order to derive a more explicit form of the scheme, we integrate the (4.2) over the rectangle $(x_{j-1/2}, x_{j+1/2}) \times (0, \Delta t)$. Since a is constant on $(x_{j-1/2}, x_{j+1/2})$, we obtain:

$$\int_{x_{j-1/2}}^{x_{j+1/2}} (U(x, \Delta t) - U(x, 0))dx + \int_0^{\Delta t} \big(F(U(x_{j+1/2} - 0, t)) - F(U(x_{j-1/2} + 0, t))\big)dt = 0. \tag{4.16}$$

Applying (4.4) and (4.14), we get:

$$\Delta x(U_j^{n+1} - U_j^n) + \int_0^{\Delta t} \big(F(U(x_{j+1/2} - 0, t)) - F(U(x_{j-1/2} + 0, t))\big)dt = 0. \tag{4.17}$$

Using the midpoint rule, we write:

$$\begin{aligned} \frac{1}{\Delta t}\int_0^{\Delta t} \big(F(U(x_{j+1/2} - 0, t))\big)dt &= F(U(x_{j+1/2} - 0, \frac{\Delta t}{2})) + O(\Delta t^2), \\ \frac{1}{\Delta t}\int_0^{\Delta t} \big(F(U(x_{j-1/2} + 0, t))\big)dt &= F(U(x_{j-1/2} + 0, \frac{\Delta t}{2})) + O(\Delta t^2). \end{aligned} \tag{4.18}$$

For approximating $F(U(x_{j+1/2} - 0, \Delta t/2))$ and $F(U(x_{j-1/2} + 0, \Delta t/2))$, we use a predictor-corrector scheme. Firstly, following an idea of Hancock, we define the updated values $U_{j+1/2,\pm}^{n+1/2}$ at time $t_n + \Delta t/2$ by

$$\begin{aligned} U_{j+1/2,-}^{n+1/2} &= U_{j+1/2,-}^n - \frac{\Delta t}{2\Delta x}(F(U_{j+1/2,-}^n) - F(U_{j-1/2,+}^n)), \\ U_{j+1/2,+}^{n+1/2} &= U_{j+1/2,+}^n - \frac{\Delta t}{2\Delta x}(F(U_{j+3/2,-}^n) - F(U_{j+1/2,+}^n)), \end{aligned} \tag{4.19}$$

where

$$\begin{aligned} U_{j+1/2,-}^n &= U_{p.lin}(x_{j+1/2} - 0) = U_j^n + \frac{1}{2}S_j^n, \\ U_{j+1/2,+}^n &= U_{p.lin}(x_{j+1/2} + 0) = U_{j+1}^n - \frac{1}{2}S_{j+1}^n. \end{aligned} \tag{4.20}$$

Secondly, we resolve the Riemann problem of (4.2) at the point $x_{j+1/2}$ with piecewise constant initial data $U_{j+1/2,\pm}^{n+1/2}$, whose solution is noted as usual

$$U_{exact}\big(\frac{x - x_{j+1/2}}{t}; U_{j+1/2,-}^{n+1/2}, U_{j+1/2,+}^{n+1/2}\big). \tag{4.21}$$

Thirdly, we replace $U(x_{j+1/2} \pm 0, \Delta t/2)$ by

$$U_{exact}\big(0\pm; U_{j+1/2,-}^{n+1/2}, U_{j+1/2,+}^{n+1/2}\big). \tag{4.22}$$

Thus, the scheme (4.17) becomes

$$U_j^{n+1} = U_j^n - \frac{\Delta t}{\Delta x}\Big(F(U_{exact}(0-; U_{j+1/2,-}^{n+1/2}, U_{j+1/2,+}^{n+1/2})) - F(U_{exact}(0+; U_{j-1/2,-}^{n+1/2}, U_{j-1/2,+}^{n+1/2}))\Big). \tag{4.23}$$

To complete the van Leer-type scheme (4.23), we will specify the values

$$\begin{aligned} U_{left} &:= U_{exact}\Big(0-; U_L, U_R\Big), \\ U_{right} &:= U_{exact}\Big(0+; U_L, U_R\Big), \end{aligned} \tag{4.24}$$

as follows:

Construction	U_{left}	U_{right}
A1 (3.1)	U_L	U_1
A2 (3.2)	U_1	U_2
A3 (3.3)	U_L	U_3
B1 (3.4)	U_1	U_2
B2 (3.5)	U_1	U_2
B3 (3.6)	U_1	U_4

(4.25)

Riemann solver (A1) The Riemann solver (A1) relying on Construction A1 yields

$$\begin{aligned} U_{exact}\Big(0-; U_L, U_R\Big) &= U_L, \\ U_{exact}\Big(0+; U_L, U_R\Big) &= U_1(U_L, U_R). \end{aligned} \tag{4.26}$$

where $U_1(U_L, U_R) = U_L^s = (h_L^s, u_L^s, \theta_L, a_R) \in \mathcal{W}_4(U_L)$, h_L^s is the smaller root of the nonlinear (2.27), $u_L^s = u_L h_L / h_L^s$.
This means that the van Leer-type scheme (4.23) using the Riemann solver (A1) is

$$U_j^{n+1} = U_j^n - \frac{\Delta t}{\Delta x}\Big(F(U_{j+1/2,-}^{n+1/2}) - F(U_1(U_{j-1/2,-}^{n+1/2}, U_{j-1/2,+}^{n+1/2}))\Big), \tag{4.27}$$

where $U_1(U_{j-1/2,-}^{n+1/2}, U_{j-1/2,+}^{n+1/2})$ is defined as in (4.26).

Riemann solver (A2) The Riemann solver (A2) relying on Construction A2 yields

$$\begin{aligned} U_{exact}\Big(0-; U_L, U_R\Big) &= U_1(U_L, U_R), \\ U_{exact}\Big(0+; U_L, U_R\Big) &= U_2(U_L, U_R). \end{aligned} \tag{4.28}$$

We can determine $U_1(U_L, U_R)$ and $U_2(U_L, U_R)$ as follows:

Step 1: Set $h_1 = h_L^{\#}$, where $h_L^{\#}$ is defined as Lemma 2.1. Set $h_2 = h^0$, where $U^0 = (h^0, u^0, \theta_L, a_L) = \mathcal{W}_1(U_L) \cap \mathcal{C}^0$.

Step 2:
- Estimate $h_T = \dfrac{h_1 + h_2}{2}$.
- Compute $U_T = (h_T, u_T, \theta_L, a_L) \in \mathcal{W}_1(U_L)$.
- Compute $U_T^b = (h_T^b, u_T^b, \theta_L, a_R) \in \mathcal{W}_4(U_T)$, where h_T^b is the bigger root of the nonlinear (2.27), $u_T^b = u_T h_T / h_T^b$.

Step 3:
- If $U_T^b \in \mathcal{W}_{3\leftarrow 2}(U_R)$, finish the computation and set $U_1(U_L, U_R) = U_T$, $U_2(U_L, U_R) = U_T^b$;
- If U_T^b is above the curve $\mathcal{W}_{3\leftarrow 2}(U_R)$, set $h_1 = h$ and return Step 2;
- If U_T^b is below the curve $\mathcal{W}_{3\leftarrow 2}(U_R)$, set $h_2 = h$ and return Step 2.

This means that the van Leer-type scheme (4.23) using the Riemann solver (A2) is

$$U_j^{n+1} = U_j^n - \frac{\Delta t}{\Delta x}\Big(F(U_1(U_{j+1/2,-}^{n+1/2}, U_{j+1/2,+}^{n+1/2})) - F(U_2(U_{j-1/2,-}^{n+1/2}, U_{j-1/2,+}^{n+1/2}))\Big), \tag{4.29}$$

where $U_1(U_{j+1/2,-}^{n+1/2}, U_{j+1/2,+}^{n+1/2})$, $U_2(U_{j-1/2,-}^{n+1/2}, U_{j-1/2,+}^{n+1/2})$ are defined as in (4.28).

Riemann solver (A3) The Riemann solver (A3) relying on Construction A3 yields

$$\begin{aligned} U_{exact}\Big(0-; U_L, U_R\Big) &= U_L, \\ U_{exact}\Big(0+; U_L, U_R\Big) &= U_3(U_L, U_R). \end{aligned} \tag{4.30}$$

We can determine $U_3(U_L, U_R)$ as follows:

Step 1: Set $a_1 = a_L, a_2 = a_R$.

Step 2:
- Estimate $a = \dfrac{a_1 + a_2}{2}$;
- Compute $U_L^s = (h_L^s, u_L^s, \theta_L, a)$ where h_L^s is the smaller root of the nonlinear (2.27), $u_L^s = u_L h_L / h_L^s$.
- Compute $U_L^{s\#} = (h_L^{s\#}, u_L^{s\#}, \theta_L, a)$ where $h_L^{s\#}, u_L^{s\#}$ are defined as Lemma 2.1.
- Compute $U_L^{s\#b} = (h_L^{s\#b}, u_L^{s\#b}, \theta_L, a_R)$ where $h_L^{s\#b}$ is the bigger root of the nonlinear (2.27), $u_L^{s\#b} = u_L^{s\#} h_L^{s\#} / h_L^{s\#b}$.

Step 3:
- If $U_L^{s\#b} \in \mathcal{W}_{3\leftarrow 2}(U_R)$, finish the computation and set $U_3(U_L, U_R) = U_L^{s\#b}$.
- If $U_L^{s\#b}$ is above the curve $\mathcal{W}_{3\leftarrow 2}(U_R)$, set $a_2 = a$ and return step 2.
- If $U_L^{s\#b}$ is below the curve $\mathcal{W}_{3\leftarrow 2}(U_R)$, set $a_1 = a$ and return step 2.

This means that the van Leer scheme (4.23) using the Riemann solver (A3) is

$$U_j^{n+1} = U_j^n - \frac{\Delta t}{\Delta x}\Big(F(U_{j+1/2,-}^{n+1/2}) - F(U_3(U_{j-1/2,-}^{n+1/2}, U_{j-1/2,+}^{n+1/2}))\Big), \tag{4.31}$$

where $U_3(U_{j-1/2,-}^{n+1/2}, U_{j-1/2,+}^{n+1/2})$ is defined as in (4.30).

Riemann solver (B1) The Riemann solver (B1) relying on Construction B1 yields

$$\begin{aligned} U_{exact}\Big(0-; U_L, U_R\Big) &= U_1(U_L, U_R), \\ U_{exact}\Big(0+; U_L, U_R\Big) &= U_2(U_L, U_R). \end{aligned} \tag{4.32}$$

where

$$\begin{aligned} U_1(U_L, U_R) &= U^+ = (h^+, u^+, \theta_L, a_L) = \mathcal{W}_1(U_L) \cap \mathcal{C}^+, \\ U_2(U_L, U_R) &= U^{+s} = (h^{+s}, u^{+s}, \theta_L, a_R). \end{aligned} \tag{4.33}$$

where h^{+s} is the smaller root of the nonlinear (2.27), $u^{+s} = u^+ h^+ / h^{+s}$.

This means that the van Leer-type scheme (4.23) using the Riemann solver (B1) is

$$U_j^{n+1} = U_j^n - \frac{\Delta t}{\Delta x}\Big(F(U_1(U_{j+1/2,-}^{n+1/2}, U_{j+1/2,+}^{n+1/2})) - F(U_3(U_{j-1/2,-}^{n+1/2}, U_{j-1/2,+}^{n+1/2}))\Big), \tag{4.34}$$

where $U_1(U^{n+1/2}_{j+1/2,-}, U^{n+1/2}_{j+1/2,+})$, $U_3(U^{n+1/2}_{j-1/2,-}, U^{n+1/2}_{j-1/2,+})$ are defined as in Eq. 4.32.

Riemann solver (B2) The Riemann solver (B2) relying on Construction B2 yields

$$\begin{aligned} U_{exact}\Big(0-; U_L, U_R\Big) &= U_1(U_L, U_R), \\ U_{exact}\Big(0+; U_L, U_R\Big) &= U_2(U_L, U_R). \end{aligned} \tag{4.35}$$

We can determine $U_1(U_L, U_R)$ and $U_2(U_L, U_R)$ as follows:

Step 1: Set $h_1 = h^+$, where $U^+ = (h^+, u^+, \theta_L, a_L) = \mathcal{W}_1(U_L) \cap \mathcal{C}^+$.
Set $h_2 = h^0$, where $U^0 = (h^0, u^0, \theta_L, a_L) = \mathcal{W}_1(U_L) \cap \mathcal{C}^0$.

Step 2:
- Estimate $h_T = \dfrac{h_1 + h_2}{2}$.
- Compute $U_T = (h_T, u_T, \theta_L, a_L) \in \mathcal{W}_1(U_L)$.
- Compute $U^b_T = (h^b_T, u^b_T, \theta_L, a_R) \in \mathcal{W}_4(U_T)$, where h^b_T is the bigger root of the nonlinear (2.27), $u^b_T = u_T h_T / h^b_T$.

Step 3:
- If $U^b_T \in \mathcal{W}_{3\leftarrow 2}(U_R)$, finish the computation and set $U_1(U_L, U_R) = U_T, U_2(U_L, U_R) = U^b_T$;
- If U^b_T is above the curve $\mathcal{W}_{3\leftarrow 2}(U_R)$, set $h_1 = h$ and return Step 2;
- If U^b_T is below the curve $\mathcal{W}_{3\leftarrow 2}(U_R)$, set $h_2 = h$ and return Step 2.

This means that the van Leer-type scheme (4.23) using the Riemann solver (B2) is

$$U^{n+1}_j = U^n_j - \frac{\Delta t}{\Delta x}\Big(F(U_1(U^{n+1/2}_{j+1/2,-}, U^{n+1/2}_{j+1/2,+})) - F(U_2(U^{n+1/2}_{j-1/2,-}, U^{n+1/2}_{j-1/2,+}))\Big), \tag{4.36}$$

where $U_1(U^{n+1/2}_{j+1/2,-}, U^{n+1/2}_{j+1/2,+})$, $U_2(U^{n+1/2}_{j-1/2,-}, U^{n+1/2}_{j-1/2,+})$ are defined as in (4.35).

Riemann solver (B3) The Riemann solver (B3) relying on Construction B3 yields

$$\begin{aligned} U_{exact}\Big(0-; U_L, U_R\Big) &= U_1(U_L, U_R), \\ U_{exact}\Big(0+; U_L, U_R\Big) &= U_4(U_L, U_R). \end{aligned} \tag{4.37}$$

We can determine $U_1(U_L, U_R)$ and $U_4(U_L, U_R)$ as follows:

Step 1: $U_1(U_L, U_R) = U^+ = (h^+, u^+, \theta_L, a_L) = \mathcal{W}_1(U_L) \cap \mathcal{C}^+$.

Step 2: Set $a_1 = a_L, a_2 = a_R$.

Step 3:
- Estimate $a = \dfrac{a_1 + a_2}{2}$;
- Compute $U^{+s} = (h^{+s}, u^{+s}, \theta_L, a)$ where h^{+s} is the smaller root of the nonlinear (2.27), $u^{+s} = u^+ h^+ / h^{+s}$.

- Compute $U^{+s\#} = (h^{+s\#}, u^{+s\#}, \theta_L, a)$ where $h^{+s\#}, u^{+s\#}$ are defined as Lemma 2.1.
- Compute $U^{+s\#b} = (h^{+s\#b}, u^{+s\#b}, \theta_L, a_R)$ where $h^{+s\#b}$ is the bigger root of the nonlinear (2.27), $u^{+s\#b} = u^{+s\#}h^{+s\#}/h^{+s\#b}$.

Step 4:
- If $U^{+s\#b} \in \mathcal{W}_{3\leftarrow 2}(U_R)$, finish the computation and set $U_4(U_L, U_R) = U^{+s\#b}$.
- If $U^{+s\#b}$ is above the curve $\mathcal{W}_{3\leftarrow 2}(U_R)$, set $a_2 = a$ and return step 3.
- If $U^{+s\#b}$ is below the curve $\mathcal{W}_{3\leftarrow 2}(U_R)$, set $a_1 = a$ and return step 3.

This means that the van Leer-type scheme (4.23) using the Riemann solver (B3) is

$$U_j^{n+1} = U_j^n - \frac{\Delta t}{\Delta x}\Big(F(U_1(U_{j+1/2,-}^{n+1/2}, U_{j+1/2,+}^{n+1/2})) - F(U_4(U_{j-1/2,-}^{n+1/2}, U_{j-1/2,+}^{n+1/2}))\Big), \tag{4.38}$$

where $U_1(U_{j+1/2,-}^{n+1/2}, U_{j+1/2,+}^{n+1/2})$, $U_4(U_{j-1/2,-}^{n+1/2}, U_{j-1/2,+}^{n+1/2})$ are defined as in (4.37).

5 Numerical tests

In this section, we will conduct the numerical experiments by using MATLAB, which demonstrate the advantage of our van Leer-type scheme (4.23) by handling either the superbee or van Leer's limiter. For each test, we compare the numerical solution U_h with the corresponding exact solution U by using the stability condition:

$$\text{CFL} = 0.5,$$

and we plot the solution U_h and U for

$$x \in [-1, 1], \quad t = 0.05.$$

Furthermore, we will compare the results of van Leer-type scheme with the outcomes of Godunov-type scheme in all of solution constructions.

5.1 Test 1: Well-balanced property

This subsection is aimed to demonstrate that our van Leer-type scheme is capable of maintaining equilibrium states as the following test cases.

5.1.1 Test 1.1: Discontinuous topography

Firstly, we conduct our van Leer-type scheme with the discontinuous topography and the initial condition in the form of

$$U_0(x) = \begin{cases} U_L = (h_L, u_L, \theta_L, a_L), & \text{if } x < 0, \\ U_R = (h_R, u_R, \theta_R, a_R), & \text{if } x > 0, \end{cases} \tag{5.1}$$

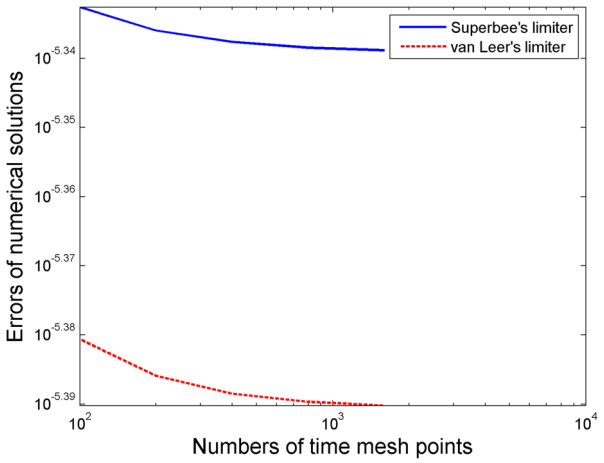

Fig. 7 A stationary contact wave is captured exactly by van Leer-type scheme using our Riemann solver with different Δt in test 1.1

where U_L, U_R are the left-hand and the right-hand states of a stationary wave, respectively. Here, they are chosen as

$$(h_L, u_L, \theta_L, a_L) = (2, 0.5, 2, 1),$$
$$(h_R, u_R, \theta_R, a_R) = (1.798490811703, 0.556021745284, 2, 1.2).$$

Figure 7 shows the errors of numerical solutions at 400 mesh points and $t = 0.05$ on the interval $[-1, 1]$ with different Δt when our scheme practices with the superbee or van Leer's limiter. Apparently, we can see that our scheme captures the stationary solutions because the errors of numerical solutions tend to zero when we increase the numbers of time mesh points, so it is well-balanced. Additionally, Table 1 also interprets this when the errors of our scheme are significantly small in the case of $\Delta t = 0.05/1600$, at only 1.9566×10^{-12}, 1.9348×10^{-12} by using the superbee and van Leer's limiters, respectively.

Table 1 Errors of numerical approximations with 400 mesh points and different Δt for test 1.1

Δt	Superbee limiter $\|\|U_h - U\|\|_{L^1}$	van Leer's limiter $\|\|U_h - U\|\|_{L^1}$
0.05/200	4.8559×10^{-12}	4.8983×10^{-12}
0.05/400	2.8548×10^{-12}	2.8098×10^{-12}
0.05/800	2.1801×10^{-12}	2.2022×10^{-12}
0.05/1600	1.9566×10^{-12}	1.9348×10^{-12}

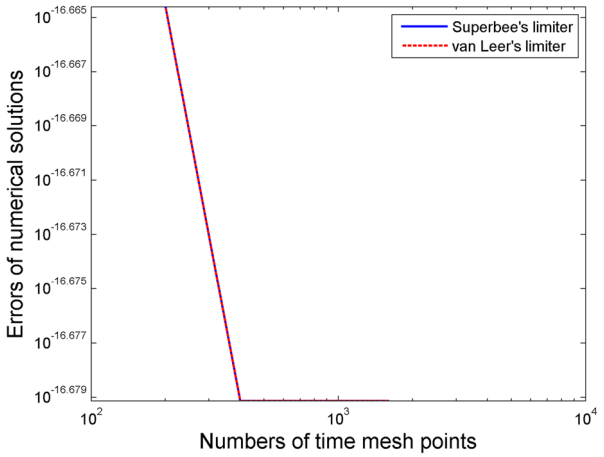

Fig. 8 A 2-contact wave with $u = 0$ is captured exactly by van Leer-type scheme using our Riemann solver with different Δt in test 1.2

5.1.2 Test 1.2: Flat topography

Secondly, we handle the problem with the flat topography and the initial condition in the form of

$$U_0(x) = \begin{cases} U_L = (h_L, u_L, \theta_L, a_L), & \text{if } x < 0, \\ U_R = (h_R, u_R, \theta_R, a_R), & \text{if } x > 0, \end{cases} \tag{5.2}$$

where U_L, U_R are the left-hand and the right-hand states of a stationary wave, respectively. Here, they are chosen as

$$\begin{aligned} (h_L, u_L, \theta_L, a_L) &= (2, 0, 0.2, 1), \\ (h_R, u_R, \theta_R, a_R) &= (2.8284, 0, 0.1, 1). \end{aligned}$$

Figure 8 represents the errors of numerical solutions at 400 mesh points and $t = 0.05$ on the interval $[-1, 1]$ with different Δt when our van Leer-type scheme operates with the superbee or van Leer's limiter. Accordingly, we can see that our scheme captures the 2-contact wave with $u = 0$ because the errors of numerical solutions reach zero when we decrease Δt, so it is well-balanced. Besides that, Table 2 also expresses this when the errors of our scheme are extremely small in the case of $\Delta t =$

Table 2 Errors of numerical approximations with 400 mesh points and different Δt for test 1.2

Δt	Superbee limiter $\|\|U_h - U\|\|_{L^1}$	van Leer's limiter $\|\|U_h - U\|\|_{L^1}$
0.05/200	2.1647×10^{-17}	2.1647×10^{-17}
0.05/400	2.0935×10^{-17}	2.0935×10^{-17}
0.05/800	2.0935×10^{-17}	2.0935×10^{-17}
0.05/1600	2.0935×10^{-17}	2.0935×10^{-17}

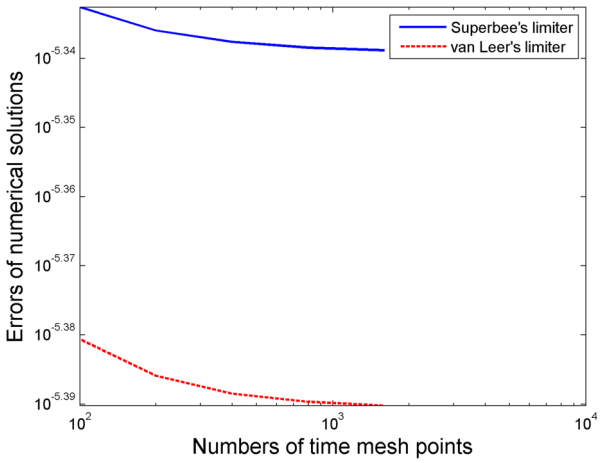

Fig. 9 A stationary contact wave is captured exactly by van Leer-type scheme using our Riemann solver with different Δt in test 1.3

0.05/1600, at only 2.0935×10^{-17}, 2.0935×10^{-17} by using the superbee and van Leer's limiters, respectively.

5.1.3 Test 1.3: Continuous topography

Thirdly, we resolve the problem with the continuous topography. Let us take the stationary solutions with the smooth topography as

$$\begin{aligned} h(x) &= \exp(x), \\ u(x) &= \exp(-x), \\ \theta(x) &= 1, \\ a(x) &= -\frac{\exp(-2x)}{2g} - \exp(x) + 3, \quad x \in [0, 1]. \end{aligned} \tag{5.3}$$

Figure 9 shows the errors of numerical solutions at 100 mesh points and $t = 0.01$ on the interval [0, 1] with different Δt when our van Leer-type scheme practices with

Table 3 Errors of numerical approximations with 100 mesh points and different Δt for test 1.3

Δt	Superbee limiter $\|\|U_h - U\|\|_{L^1}$	van Leer's limiter $\|\|U_h - U\|\|_{L^1}$
0.01/100	4.6494×10^{-6}	4.1627×10^{-6}
0.01/200	4.6135×10^{-6}	4.1126×10^{-6}
0.01/400	4.5959×10^{-6}	4.0883×10^{-6}
0.01/800	4.5872×10^{-6}	4.0773×10^{-6}
0.01/1600	4.5833×10^{-6}	4.0721×10^{-6}

Table 4 Errors of numerical approximations with 100 mesh points and different t for test 1.3

t	Superbee limiter $\|\|U_h - U\|\|_{L^1}$	van Leer's limiter $\|\|U_h - U\|\|_{L^1}$
0.01	5.6314×10^{-6}	5.4015×10^{-6}
0.001	6.3595×10^{-7}	6.1646×10^{-7}
0.0001	4.8140×10^{-8}	4.5478×10^{-8}
0.00001	4.6111×10^{-9}	4.3433×10^{-9}
0.000001	4.5908×10^{-10}	4.3234×10^{-10}

the superbee or van Leer's limiter. Clearly, we can see that our scheme captures the smooth stationary solutions because the errors of numerical solutions tend to zero when the numbers of time mesh points get bigger, so it is well-balanced. Besides that, Table 3 also points out this when the error of our scheme is really small in the case of $\Delta t = 0.01/1600$, at only 4.5833×10^{-6}, 4.0721×10^{-6} by using the superbee and van Leer's limiters, respectively. The errors decrease slowly because there is an accumulation of ones, so the errors of stationary solutions get sharply small when the time gets small. Moreover, this issue is also pointed out in Table 4 and Fig. 10.

5.1.4 Test 1.4: Stationary solutions of form $u = 0, [h] = 0, [2a + h\ln(\theta)] = 0$.

It is derived from (2.24) that a smooth stationary solution of (1.1) can be determined by the equations

$$u = 0, \quad h' = 0, \quad (2a + h\ln(\theta))' = 0,$$

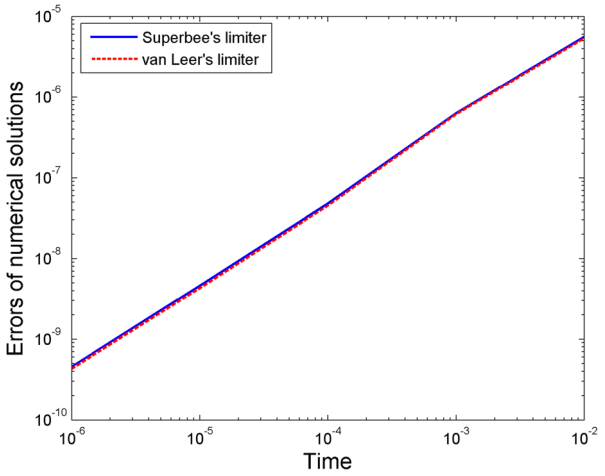

Fig. 10 A stationary contact wave is captured exactly by van Leer-type scheme using our Riemann solver with different t in test 1.3

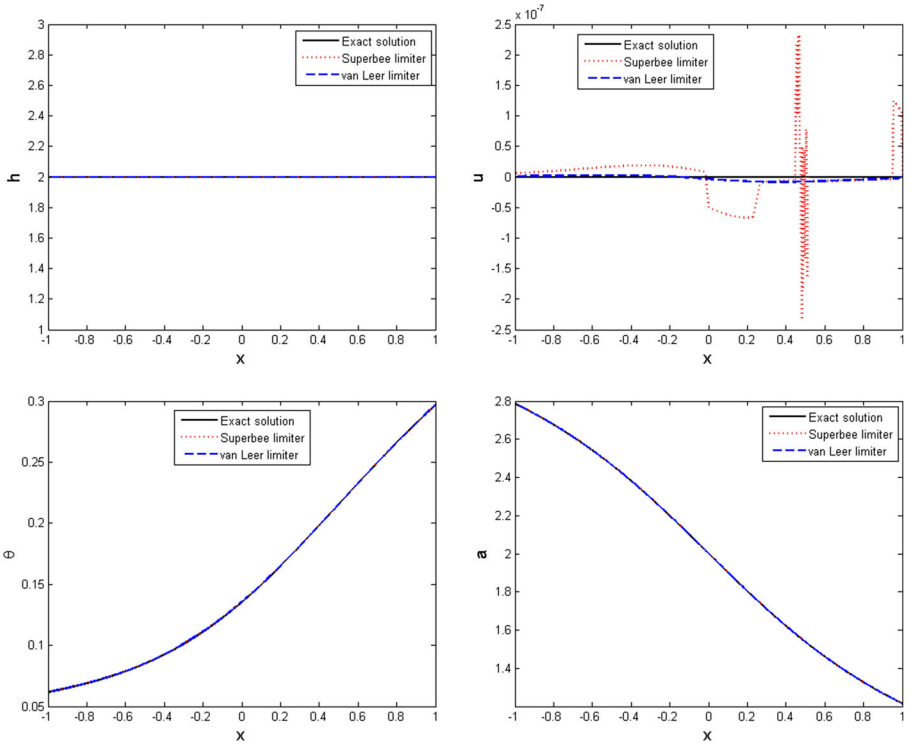

Fig. 11 Exact and approximate solutions with 800 mesh points for test 1.4 with smooth initial data (5.4)

where $(.)' = d(.)/dx$; see [13]. By an approximation argument, a steady-state discontinuity of the form

$$u = 0, \quad [h] = 0, \quad [2a + h\ln(\theta)] = 0,$$

is also a weak solution of (1.1). In this test, we aim to show that our scheme (4.23) can capture this kind of stationary solutions in both cases of smooth solutions and steady-state discontinuity.

Indeed, let us first consider the Cauchy problem for (1.1) with the smooth initial data $U_0(x) = (h(x), u(x), \theta(x), a(x))$, where

$$\begin{aligned} h(x) &= 2, \\ u(x) &= 0, \\ \theta(x) &= \exp(-2 + \arctan(x)), \\ a(x) &= 2 - \arctan(x), \end{aligned} \tag{5.4}$$

and with the discontinuous initial data

$$U_0(x) = \begin{cases} (h_L, u_L, \theta_L, a_L) = (0.7, 0, 2, 1.5), \\ (h_R, u_R, \theta_R, a_R) = (0.7, 0, 2.30712998979022, 1.45). \end{cases} \tag{5.5}$$

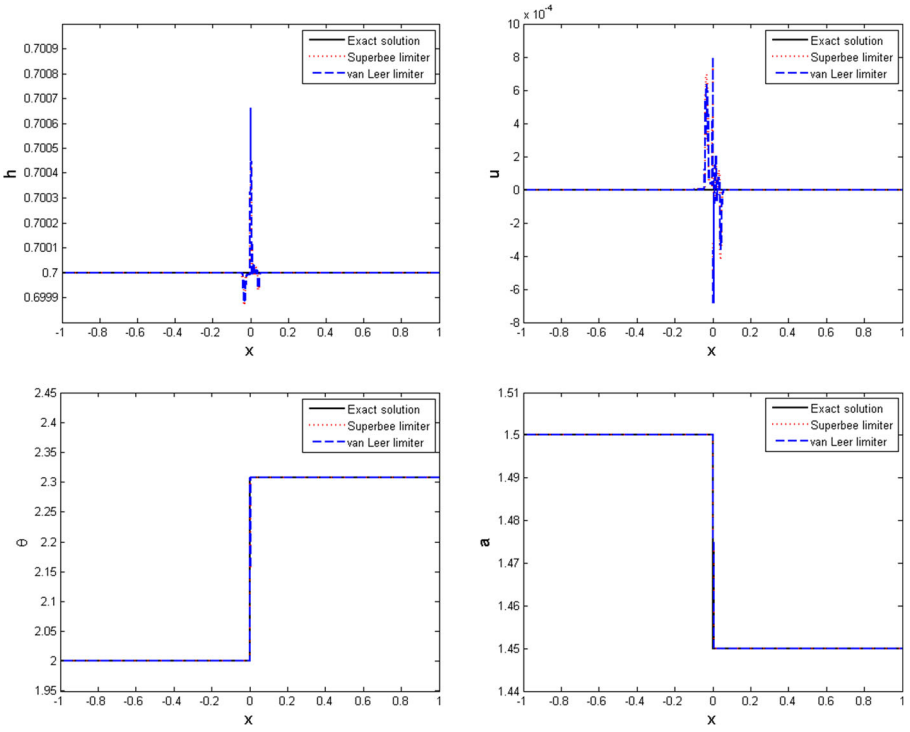

Fig. 12 Exact and approximate solutions with 800 mesh points for test 1.4 with discontinuous initial data Eq. 5.5

The exact solutions of these test are stationary solutions $U(x,t) = U_0(x)$, $x \in \mathbb{R}$, $t \geq 0$.

Figures 11 and 12 show the exact solutions and their approximations by the scheme (4.23) for this test with smooth and discontinuous initial data at time $t = 0.01$ on the interval $[-1, 1]$ with 800 mesh points, respectively. Figures 13 and 14 express the errors of numerical solutions with different mesh points when our van Leer-type scheme practices with the superbee or van Leer's limiter. These figures and Tables 5 and 6 show that our scheme can approximate this kind of stationary solutions with a very high accuracy in both cases. More precisely, the scheme can capture almost exactly the smooth solution, but has some small oscillations near the discontinuity.

5.2 Test 2: Construction A1

In this test, we conduct to approximate a Riemann solution of Construction A1. The Riemann data are given by

$$U_0(x) = \begin{cases} U_L = (h_L, u_L, \theta_L, a_L) = (0.01, 3, 2, 1.2) \in G_1, & \text{if } x < 0, \\ U_R = (h_R, u_R, \theta_R, a_R) = (0.02, 2, 3, 1) \in G_1, & \text{if } x > 0. \end{cases} \tag{5.6}$$

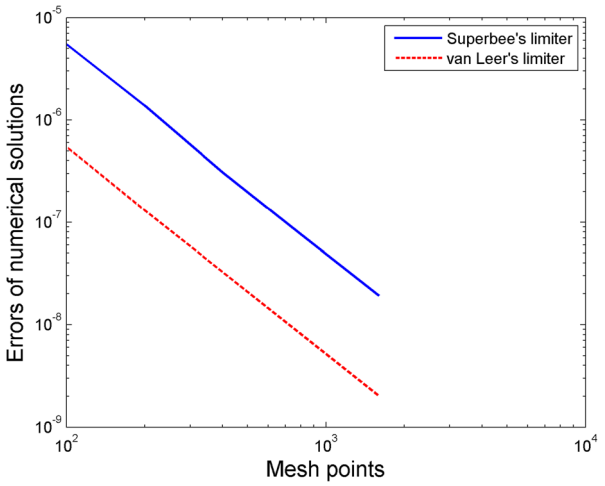

Fig. 13 Steady smooth solution of form $u = 0, [h] = 0, [2a + h\ln(\theta)] = 0$ in test 1.4 is captured by van Leer-type scheme (4.23)

According to Construction A1, the exact solution is started by a stationary wave from U_L to U_1, then followed by a 1-shock wave from U_1 to U_2, then followed by a 2-contact wave from U_2 to U_3, then followed by a 3-shock wave from U_3 to U_R, where U_L, U_1, U_2, U_3, and U_R are reported in Table 7.

Figure 15 shows an exact solutions and its approximation at time $t = 0.05$ on the interval $[-1, 1]$ with 100 mesh points by the van Leer-type scheme using the superbee or van Leer's limiter and the Godunov-type scheme. Besides that, the errors

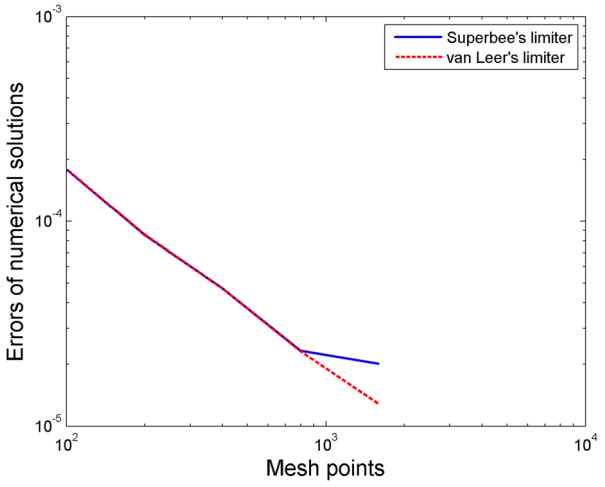

Fig. 14 Steady discontinuous solution of form $u = 0, [h] = 0, [2a + h\ln(\theta)] = 0$ in test 1.4 is captured by van Leer-type scheme (4.23)

Table 5 Errors of numerical approximations with different mesh points for test 1.4 with smooth initial data Eq. 5.4

N	Superbee limiter $\|\|U_h - U\|\|_{L^1}$	van Leer's limiter $\|\|U_h - U\|\|_{L^1}$
100	5.51×10^{-6}	5.4914×10^{-7}
200	1.3836×10^{-6}	1.3134×10^{-7}
400	3.0632×10^{-7}	3.2655×10^{-8}
800	7.6038×10^{-8}	8.1013×10^{-9}
1600	1.9247×10^{-8}	2.0197×10^{-9}

of solutions and orders of accuracy for test 2 are reported in Table 8 and the errors of solutions are also presented in Fig. 16.

Looking at Table 8 and Fig. 16, we are able to see that the approximate solutions of both schemes in comparison with exact solutions get smaller when the mesh sizes get smaller, yet the errors of van Leer-type scheme are much smaller than the ones of Godunov-type scheme. In addition, the orders of accuracy of van Leer-type scheme are higher than the ones of Godunov-type scheme. Furthermore, it is easy to observe that the graph of approximate solutions of van Leer-type scheme using the superbee limiter is closer to the graph of exact solutions than the one of van Leer-type scheme using van Leer's limiter and of Godunov-type scheme as in Fig. 15.

Thus, this test demonstrates the convergence of the approximate solutions by van Leer-type scheme to the exact solutions. Especially, the accuracy of the van Leer-type scheme using the superbee limiter is better than the one using the van Leer's limiter.

5.3 Test 3: Construction A2

In this test, we conduct approximating a Riemann solution of Construction A2. We consider the Riemann data to be

$$U_0(x) = \begin{cases} U_L = (h_L, u_L, \theta_L, a_L) = (0.5, 4, 3, 1.5) \in G_1, & \text{if } x < 0, \\ U_R = (h_R, u_R, \theta_R, a_R) = (1.2, 1.5, 4, 1) \in G_2, & \text{if } x > 0. \end{cases} \tag{5.7}$$

Table 6 Errors of numerical approximations with different mesh points for test 1.4 with discontinuous initial data (5.5)

N	Superbee limiter $\|\|U_h - U\|\|_{L^1}$	van Leer's limiter $\|\|U_h - U\|\|_{L^1}$
100	1.7945×10^{-4}	1.8037×10^{-4}
200	8.5315×10^{-5}	8.5911×10^{-5}
400	4.7037×10^{-5}	4.6888×10^{-5}
800	2.3314×10^{-5}	2.3156×10^{-5}
1600	2.0166×10^{-5}	1.2822×10^{-5}

Table 7 States that separate the elementary waves of the exact solution of the Riemann problem in test 2: Construction A1

	U_L	U_1	U_2	U_3	U_R
h	0.01	0.007287	0.045991	0.037551	0.02
u	3.0	4.116756	2.589118	2.589118	2.0
θ	2.0	2.0	2.0	3.0	3.0
a	1.2	1.0	1.0	1.0	1.0

According to construction A2, the exact solution is started by a 1-shock wave from U_L to U_1, then followed by a stationary wave from U_1 to U_2, then followed by a 2-contact wave from U_2 to U_3, then followed by a 3-rarefaction wave from U_3 to U_R, where U_L, U_1, U_2, U_3, and U_R are reported in Table 9.

Figures 17 and 18 represents an exact solution and its approximation at time $t = 0.05$ on the interval $[-1, 1]$ with 100 and 1600 mesh points, respectively by the van Leer-type scheme using the superbee or van Leer's limiter and the Godunov-type scheme. Besides that, the errors of solution and orders of accuracy for test 3 are reported in the Table 10 and the errors of solutions are also presented in Fig. 19.

Table 10 and Fig. 19 point out that the errors of three schemes become smaller when the mesh sizes get smaller, and the errors of van Leer-type scheme are the

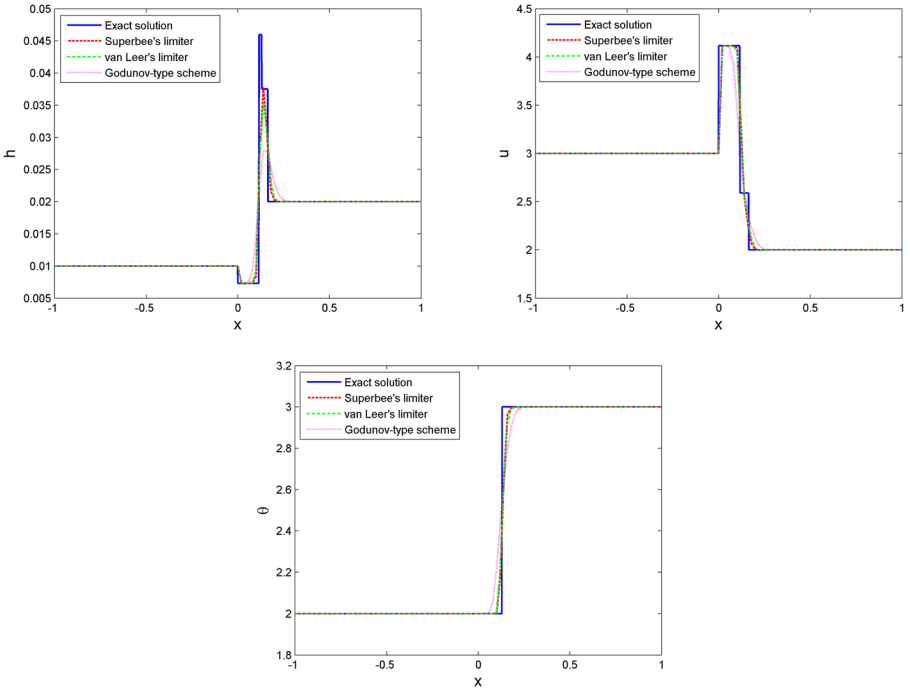

Fig. 15 Exact and approximate solutions with 100 mesh points for test 2

Table 8 Errors of numerical approximations and orders of accuracy for different mesh sizes for test 2

	Godunov-type scheme		Superbee limiter		van Leer's limiter	
N	$\|\|U_h - U\|\|_{L^1}$	Order	$\|\|U_h - U\|\|_{L^1}$	Order	$\|\|U_h - U\|\|_{L^1}$	Order
100	0.0844		0.0484		0.0505	
200	0.0588	0.52	0.0253	0.94	0.0300	0.75
400	0.0395	0.57	0.0164	0.63	0.0191	0.66
800	0.0235	0.75	0.0076	1.10	0.0093	1.03
1600	0.0145	0.69	0.0038	1.00	0.0050	0.89
3200	0.0092	0.66	0.0022	0.83	0.0028	0.84
6400	0.0059	0.64	0.0011	0.91	0.0016	0.85

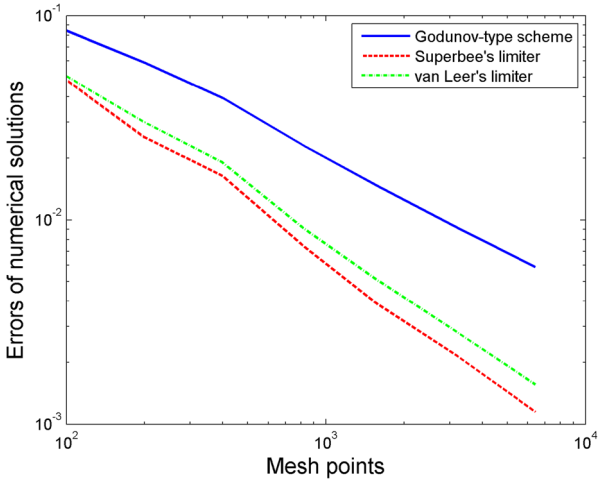

Fig. 16 Errors of numerical solutions with different mesh points for test 2

Table 9 States that separate the elementary waves of the exact solution of the Riemann problem in test 3: Construction A2

	U_L	U_1	U_2	U_3	U_R
h	0.5	0.780210	1.327153	1.149348	1.2
u	4.0	2.053781	1.207381	1.207381	1.5
θ	3.0	3.0	3.0	4.0	4.0
a	1.5	1.5	1.0	1.0	1.0

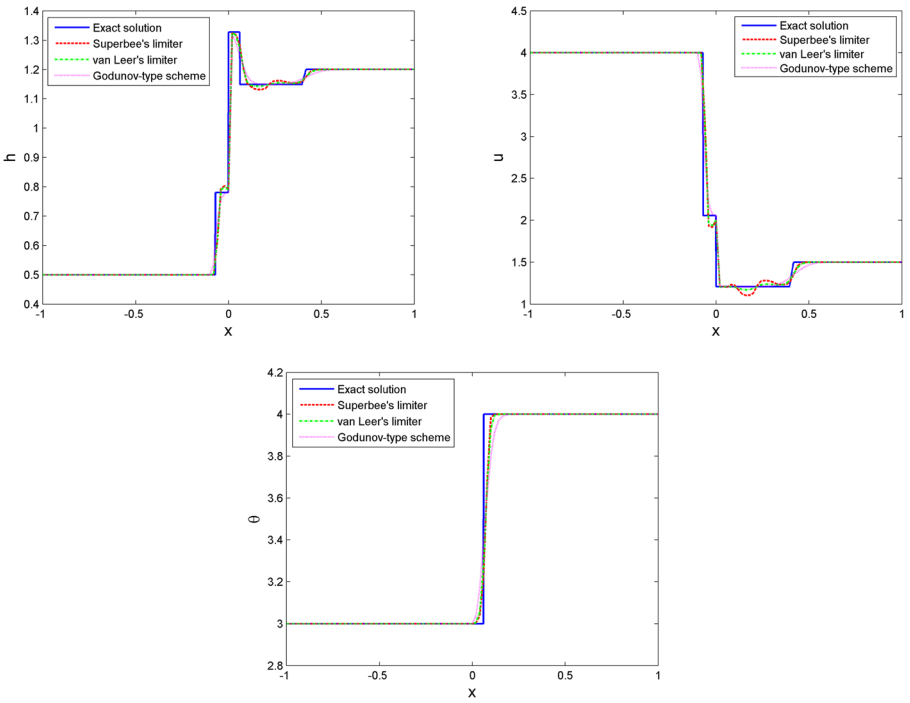

Fig. 17 Exact and approximate solutions with 100 mesh points for test 3

smallest. In addition, the orders of accuracy of van Leer-type scheme are the highest; and we also see these results as in Table 11 and Fig. 20 when we consider on the interval $(0.3970, 0.4169)$ containing rarefaction wave. Furthermore, the van Leer-type scheme using the superbee limiter has slightly higher orders of accuracy than the one using van Leer's limiter as in Table 10.

However, we observe that the graph of approximate solutions of van Leer-type scheme using the superbee limiter is closer to the graph of exact solutions than the

Table 10 Errors of numerical approximations and orders of accuracy for different mesh sizes for test 3

	Godunov-type scheme		Superbee limiter		van Leer's limiter	
N	$\|\|U_h - U\|\|_{L^1}$	Order	$\|\|U_h - U\|\|_{L^1}$	Order	$\|\|U_h - U\|\|_{L^1}$	Order
100	0.1016		0.1025		0.0942	
200	0.0672	0.60	0.0584	0.81	0.0561	0.75
400	0.0371	0.86	0.0237	1.30	0.0235	1.25
800	0.0232	0.68	0.0113	1.07	0.0118	1.00
1600	0.0152	0.62	0.0054	1.06	0.0061	0.95
3200	0.0100	0.60	0.0033	0.71	0.0038	0.69
6400	0.0068	0.56	0.0021	0.67	0.0024	0.66

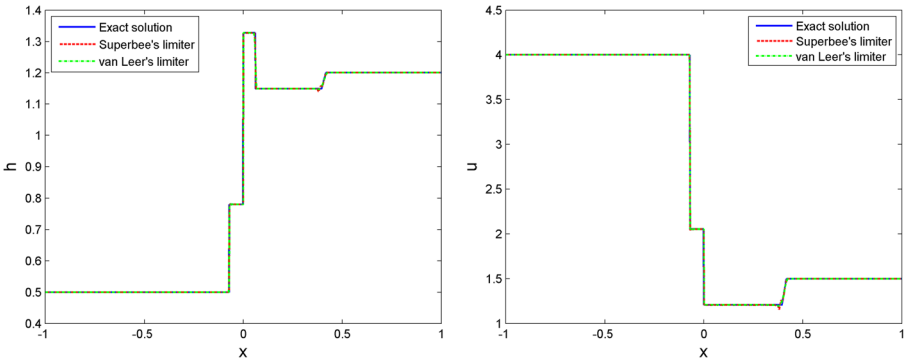

Fig. 18 Exact and approximate solutions with 1600 mesh points for test 3

one of van Leer-type scheme using van Leer's limiter and of Godunov-type scheme as in Fig. 17, except the left hand of the stationary wave $\mathcal{W}_4(U_1, U_2)$ and of the 3-rarefaction wave $\mathcal{R}_3(U_3, U_R)$ in the first two pictures of h, u in Fig. 17. If the mesh size is reduced to $h = 2/1600$, then the oscillations of graph of numerical solutions are quite tiny on the left hand of the 3-rarefaction wave $\mathcal{R}_3(U_3, U_R)$, and almost disappears on the left hand of stationary wave $\mathcal{W}_4(U_1, U_2)$ as shown in Fig. 19.

Consequently, test 3 demonstrates the convergence of the approximate solutions by van Leer-type scheme to the exact solution when the initial data belong to supercritical and subcritical. Although the van Leer-type scheme using the superbee limiter has a better accuracy than using the van Leer's limiter, it suffers a slight oscillation around the approximation of the 3-rarefaction wave $\mathcal{R}_3(U_3, U_R)$ in Fig. 17.

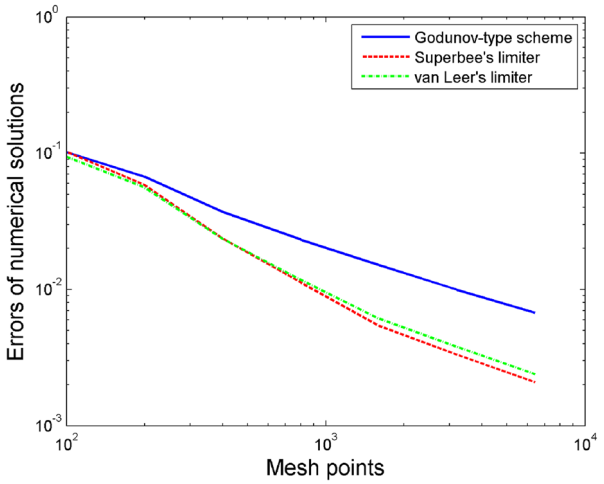

Fig. 19 Errors of numerical solutions with different mesh points for test 3

Table 11 Errors of numerical approximations and orders of accuracy for different mesh sizes for test 3 in the interval of rarefaction wave (0.3970, 0.4169)

	Godunov-type scheme		Superbee limiter		van Leer's limiter	
N	$\|\|U_h - U\|\|_{L^1}$	Order	$\|\|U_h - U\|\|_{L^1}$	Order	$\|\|U_h - U\|\|_{L^1}$	Order
1600	6.6817×10^{-4}		2.5273×10^{-4}		2.3510×10^{-4}	
3200	6.6135×10^{-4}	0.01	1.6083×10^{-4}	0.65	1.6368×10^{-4}	0.52
6400	5.6432×10^{-4}	0.23	1.1038×10^{-4}	0.54	1.0204×10^{-4}	0.68

5.4 Test 4: Construction A3

In this test, we conduct to approximate a Riemann solution of Construction A3, where the Riemann data are given by

$$U_0(x) = \begin{cases} U_L = (h_L, u_L, \theta_L, a_L) = (0.5, 4, 3, 1.5) \in G_1, & \text{if } x < 0, \\ U_R = (h_R, u_R, \theta_R, a_R) = (1.1, 3.2, 4, 1) \in G_2, & \text{if } x > 0. \end{cases} \tag{5.8}$$

According to Construction A3, the exact solution is started by a stationary wave from U_L to U_1, then followed by a 1-shock wave with zero-speed from U_1 to U_2, then followed by a stationary wave from U_2 to U_3, then followed by a 2-contact wave from U_3 to U_4, then followed by a 3-rarefaction wave from U_4 to U_R, where $U_L, U_1, U_2, U_3, U_4, U_R$ are reported in Table 12.

One can see from the configuration of the exact solution (3.3) that the exact solution contains three waves propagating with the same zero speed.

Figure 21 expresses an exact solution and its approximation at time $t = 0.05$ on the interval $[-1, 1]$ with 100 mesh points by the van Leer-type scheme using the

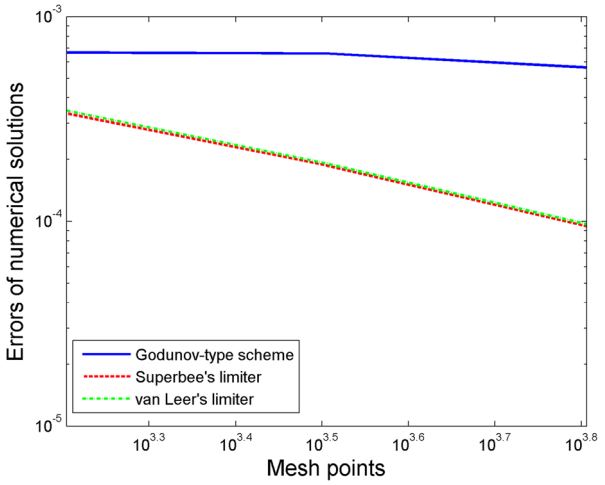

Fig. 20 Errors of numerical solutions with different mesh points in the interval of rarefaction wave for test 3

Table 12 States that separate the elementary waves of the exact solution of the Riemann problem in test 4: Construction A3

	U_L	U_1	U_2	U_3	U_4	U_R
h	0.5	0.288128	0.838361	1.036362	0.897516	1.1
u	4.0	6.941370	2.385607	1.929828	1.929828	3.2
θ	3.0	3.0	3.0	3.0	4.0	4.0
a	1.5	1.164550	1.164550	1.0	1.0	1.0

superbee limiter or van Leer's limiter and the Godunov-type scheme. Besides that, the errors of solution and orders of accuracy for test 4 are reported in Table 13 and the errors of solutions are also showed in Fig. 22.

Table 13 and Fig. 22 show that the errors for approximating solutions of both schemes become smaller when the mesh sizes get smaller, and that the errors of van Leer-type scheme are much smaller than the ones of Godunov-type scheme. In addition, the orders of accuracy of van Leer-type scheme are higher than the ones of Godunov-type scheme; and we also see these outcomes as in Table 14 and Fig. 23

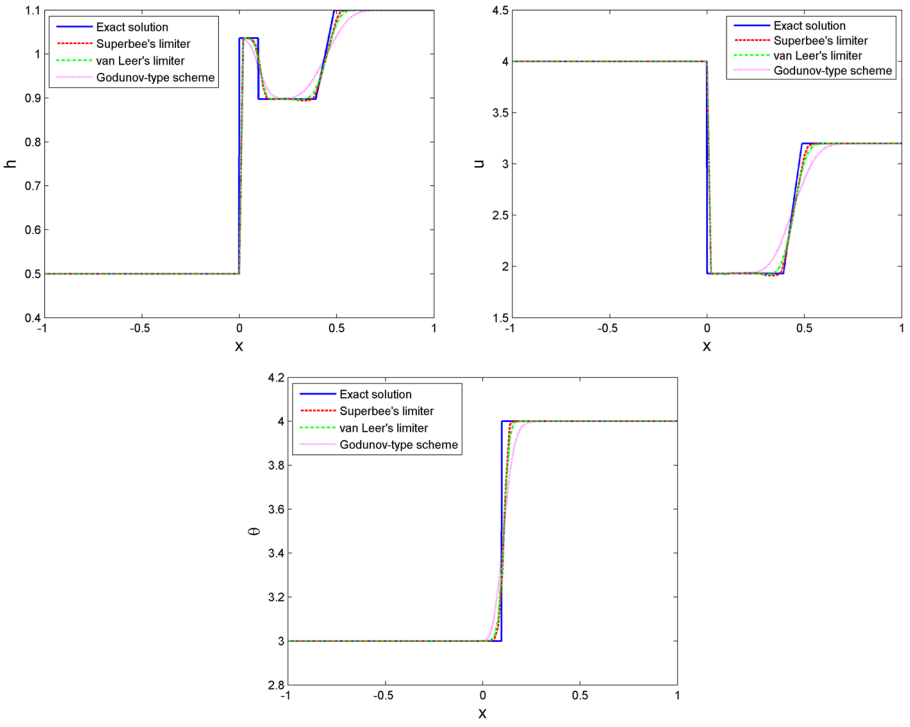

Fig. 21 Exact and approximate solutions with 100 mesh points for test 4

Table 13 Errors of numerical approximations and orders of accuracy for different mesh sizes for test 4

	Godunov-type scheme		Superbee limiter		van Leer's limiter	
N	$\|\|U_h - U\|\|_{L^1}$	Order	$\|\|U_h - U\|\|_{L^1}$	Order	$\|\|U_h - U\|\|_{L^1}$	Order
100	0.1540		0.0863		0.0945	
200	0.0956	0.69	0.0399	1.11	0.0469	0.75
400	0.0605	0.66	0.0195	1.04	0.0242	1.25
800	0.0389	0.64	0.0106	0.88	0.0135	1.00
1600	0.0247	0.65	0.0051	1.04	0.0070	0.95
3200	0.0158	0.65	0.0027	0.90	0.0039	0.84
6400	0.0101	0.65	0.0015	0.87	0.0022	0.83

when we consider on the interval (0.4181, 0.4633) containing rarefaction wave, the tendency of the orders of accuracy gradually increase in case the mesh points get bigger. Furthermore, it is easy to observe that the graph of approximate solutions of van Leer-type scheme using the superbee limiter is closer to the graph of exact solutions than the one of van Leer-type scheme using van Leer's limiter and of Godunov-type scheme as in Fig. 21.

This test also demonstrates the convergence of the approximate solutions by van Leer-type scheme to the exact solution when the initial data *even for the resonant phenomenon*, where several waves travel with a coinciding speed. Especially, the approximate solutions by the van Leer-type scheme using the superbee limiter are closer to the exact solutions than the one using the van Leer's limiter.

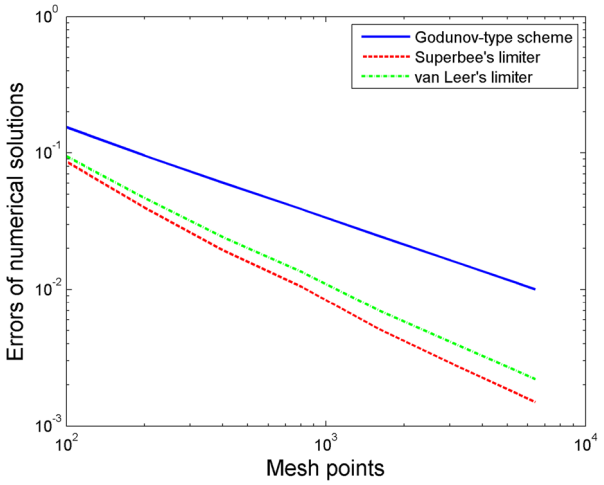

Fig. 22 Errors of numerical solutions with different mesh points for test 4

Table 14 Errors of numerical approximations and orders of accuracy for different mesh sizes for test 4 in the interval of rarefaction wave (0.4181, 0.4633)

	Godunov-type scheme		Superbee limiter		van Leer's limiter	
N	$\|\|U_h - U\|\|_{L^1}$	Order	$\|\|U_h - U\|\|_{L^1}$	Order	$\|\|U_h - U\|\|_{L^1}$	Order
200	0.0023		0.0017		0.0017	
400	0.0020	0.17	0.0011	0.68	0.0011	0.66
800	0.0016	0.38	5.9980×10^{-4}	0.85	6.2033×10^{-4}	0.84
1600	0.0012	0.37	3.3539×10^{-4}	0.84	3.4589×10^{-4}	0.84
3200	8.5948×10^{-4}	0.51	1.8674×10^{-4}	0.85	1.9099×10^{-4}	0.86
6400	5.0177×10^{-4}	0.78	9.4428×10^{-5}	0.98	9.6710×10^{-5}	0.98

5.5 Test 5: Construction B1

In this test, we conduct to approximate a Riemann solution of Construction B1 with the Riemann data:

$$U_0(x) = \begin{cases} U_L = (h_L, u_L, \theta_L, a_L) = (0.5, 1, 3, 1.5) \in G_2, & \text{if } x < 0, \\ U_R = (h_R, u_R, \theta_R, a_R) = (0.3, 4, 2, 1.3) \in G_1, & \text{if } x > 0. \end{cases} \tag{5.9}$$

According to Construction B1, the exact solution is started by a 1-rarefaction wave from U_L to U_1, then followed by a stationary wave from U_1 to U_2, then followed by a 1-shock wave from U_2 to U_3, then followed by a 2-contact wave from U_3 to U_4, then followed by a 3-shock wave from U_4 to U_R, where U_L, U_1, U_2, U_3, U_4, and U_R are reported in Table 15.

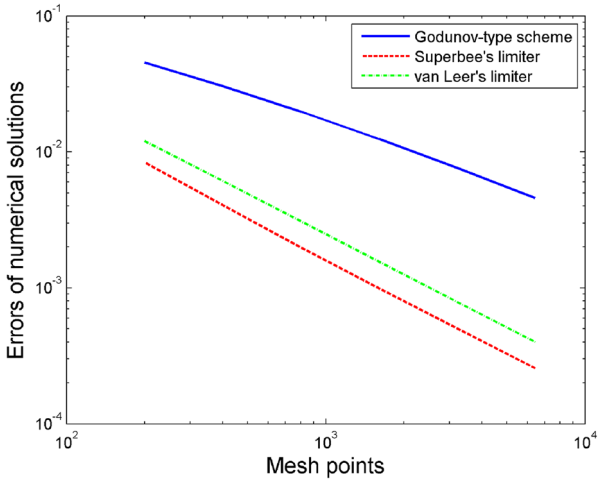

Fig. 23 Errors of numerical solutions with different mesh points in the interval of rarefaction wave for test 4

Table 15 States that separate the elementary waves of the exact solution of the Riemann problem in test 5: Construction B1

	U_L	U_1	U_2	U_3	U_4	U_R
h	0.5	0.283962	0.156098	0.252118	0.308780	0.3
u	1.0	2.889365	5.256126	4.070455	4.070455	4.0
θ	3.0	3.0	3.0	3.0	2.0	2.0
a	1.5	1.5	1.3	1.3	1.3	1.3

Figures 24 and 25 represents an exact solutions and its approximation at time $t = 0.05$ on the interval $[-1, 1]$ with 100 and 1600 mesh points, respectively by the van Leer-type scheme using the superbee or van Leer's limiter and the Godunov-type scheme. Besides that, the errors of solution and orders of accuracy for test 5 are reported in Table 16 and the errors of solutions are also showed in Fig. 26.

Table 16 and Fig. 26 also demonstrate the convergence of both schemes, and the errors of van Leer-type scheme are much smaller than the ones of Godunov-type scheme. Again, the orders of accuracy of van Leer-type scheme are higher than the ones of Godunov-type scheme; and we also have the similar results as in Table 17 and

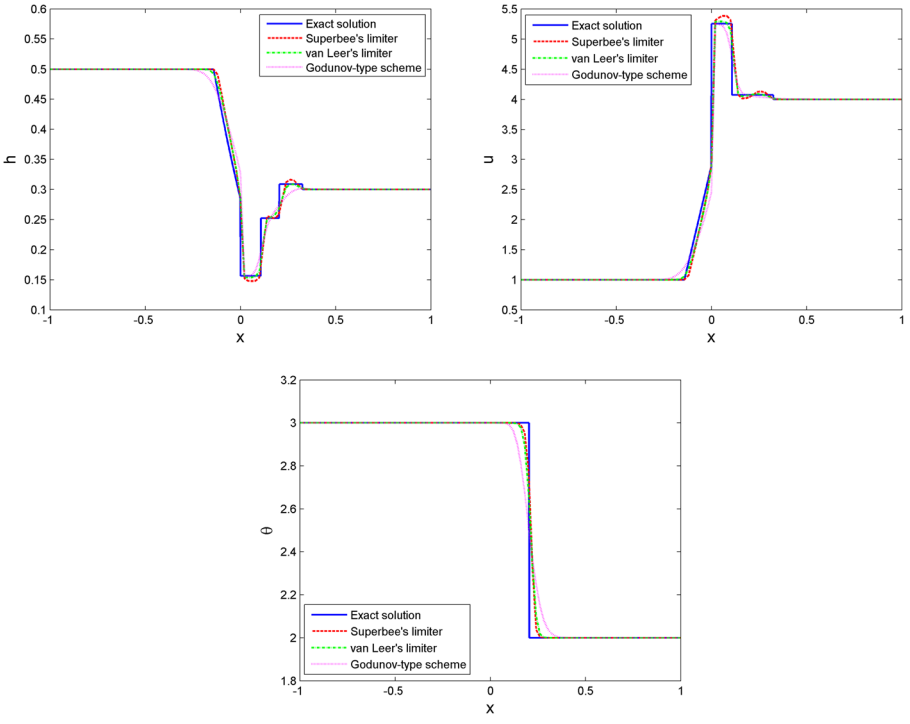

Fig. 24 Exact and approximate solutions with 100 mesh points for test 5

Table 16 Errors of numerical approximations and orders of accuracy for different mesh sizes for test 5

	Godunov-type scheme		Superbee limiter		van Leer's limiter	
N	$\|\|U_h - U\|\|_{L^1}$	Order	$\|\|U_h - U\|\|_{L^1}$	Order	$\|\|U_h - U\|\|_{L^1}$	Order
100	0.1635		0.1043		0.0992	
200	0.1024	0.67	0.0650	0.68	0.0593	0.74
400	0.0630	0.70	0.0292	1.16	0.0289	1.04
800	0.0396	0.67	0.0162	0.85	0.0172	0.75
1600	0.0245	0.69	0.0078	1.05	0.0085	1.01
3200	0.0155	0.66	0.0035	1.16	0.0043	0.99
6400	0.0099	0.64	0.0021	0.76	0.0026	0.74

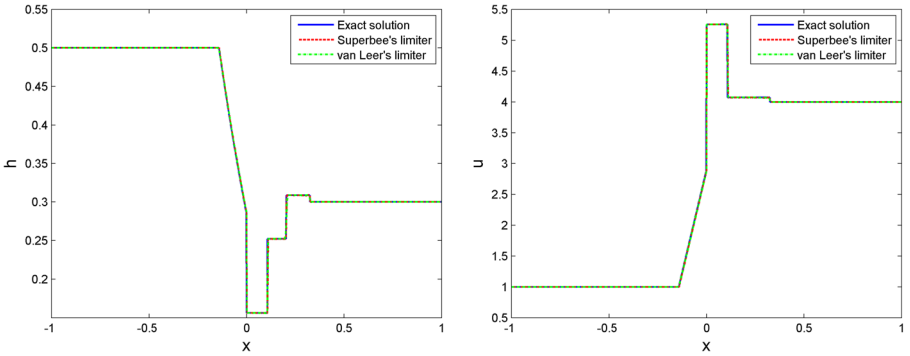

Fig. 25 Exact and approximate solutions with 1600 mesh points for test 5

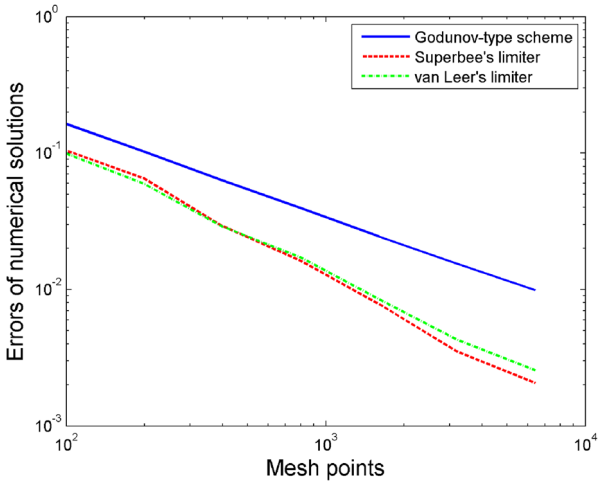

Fig. 26 Errors of numerical solutions with different mesh points for test 5

Table 17 Errors of numerical approximations and orders of accuracy for different mesh sizes for test 5 in the interval of rarefaction wave $(-0.1317, 0.0000)$

	Godunov-type scheme		Superbee limiter		van Leer's limiter	
N	$\|\|U_h - U\|\|_{L^1}$	Order	$\|\|U_h - U\|\|_{L^1}$	Order	$\|\|U_h - U\|\|_{L^1}$	Order
200	0.0139		0.0113		0.0099	
400	0.0109	0.35	0.0065	0.81	0.0058	0.76
800	0.0073	0.58	0.0034	0.92	0.0031	0.89
1600	0.0046	0.66	0.0018	0.93	0.0017	0.92
3200	0.0027	0.78	9.0197×10^{-4}	0.99	8.3105×10^{-4}	0.99
6400	0.0016	0.79	4.5603×10^{-4}	0.98	4.2091×10^{-4}	0.98

Fig. 27 when we consider on the interval $(-0.1317, 0.0000)$ containing rarefaction wave.

Nevertheless, the van Leer-type scheme using the superbee limiter suffers a small oscillation around the 1-shock wave $\mathcal{S}_1(U_2, U_3)$ of the first two pictures of h, u in Fig. 24. If the mesh sizes are reduced with 1600 mesh points on $[-1, 1]$, then this oscillation almost disappears; see Fig. 25.

Thus, this test also shows the convergence of the approximate solutions by the van Leer-type scheme to the exact solution. Especially, the approximate solutions of our scheme using the superbee limiter reach the exact solutions better than the van Leer's ones.

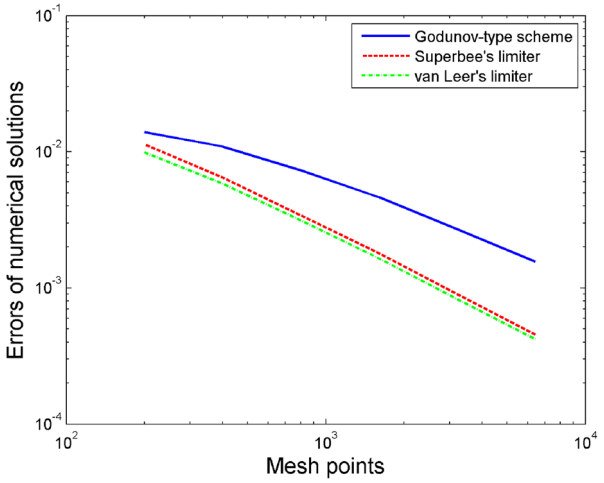

Fig. 27 Errors of numerical solutions with different mesh points in the interval of rarefaction wave for test 5

Table 18 States that separate the elementary waves of the exact solution of the Riemann problem in test 6: Construction B2

	U_L	U_1	U_2	U_3	U_R
h	0.6	0.518204	1.156671	1.335608	1.5
u	3.0	3.685363	1.651092	1.651092	2.4
θ	4.0	4.0	4.0	3.0	3.0
a	1.5	1.5	1.0	1.0	1.0

5.6 Test 6: Construction B2

In this test, we conduct approximating a Riemann solution of Construction B2 with the Riemann data:

$$U_0(x) = \begin{cases} U_L = (h_L, u_L, \theta_L, a_L) = (0.6, 3, 4, 1.5) \in G_2, & \text{if } x < 0, \\ U_R = (h_R, u_R, \theta_R, a_R) = (1.5, 2.4, 3, 1) \in G_2, & \text{if } x > 0. \end{cases} \tag{5.10}$$

According to Construction B2, the exact solution is started by a 1-rarefaction wave from U_L to U_1, then followed by a stationary wave from U_1 to U_2, then followed by

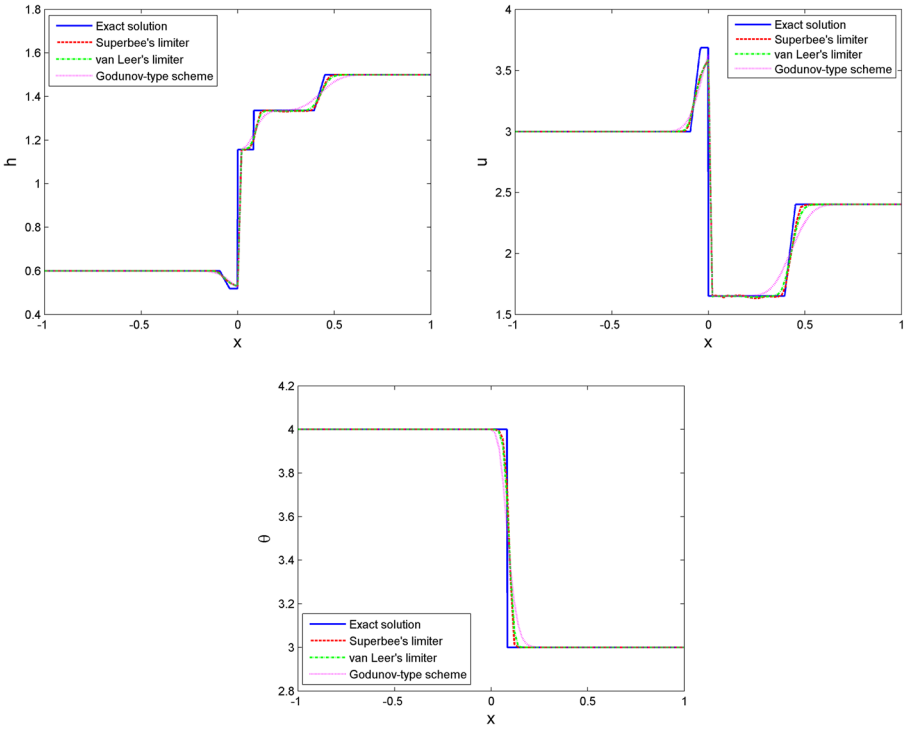

Fig. 28 Exact and approximate solutions with 100 mesh points for test 6

Table 19 Errors of numerical approximations and orders of accuracy for different mesh sizes for test 6

	Godunov-type scheme		Superbee limiter		van Leer's limiter	
N	$\|\|U_h - U\|\|_{L^1}$	Order	$\|\|U_h - U\|\|_{L^1}$	Order	$\|\|U_h - U\|\|_{L^1}$	Order
100	0.1399		0.0815		0.0904	
200	0.0906	0.63	0.0436	0.90	0.0499	0.86
400	0.0579	0.65	0.0226	0.94	0.0269	0.89
800	0.0374	0.63	0.0108	1.06	0.0139	0.96
1600	0.0241	0.63	0.0055	0.98	0.0074	0.90
3200	0.0156	0.63	0.0028	1.00	0.0040	0.89
6400	0.0100	0.63	0.0014	0.99	0.0022	0.87

a 2-contact wave from U_2 to U_3, then followed by a 3-rarefaction wave from U_3 to U_R, where U_L, U_1, U_2, U_3, and U_R are reported in Table 18.

The exact and approximate solutions at time $t = 0.05$ with 100 mesh points on the interval $[-1, 1]$ are displayed in Fig. 28. The errors and orders of accuracy are reported in Tables 19, 20, and 21, and the errors of solutions are also showed in Figs. 29, 30, and 31.

The approximate solutions are shown to be convergent to the exact solution, by Table 19 and Fig. 29. And, the errors of van Leer-type scheme are much smaller than the ones of Godunov-type scheme. In addition, the orders of accuracy of van Leer-type scheme are higher than the ones of Godunov-type scheme. Our van Leer-type scheme using the superbee limiter has the best orders of accuracy among the three tested ones.

5.7 Test 7: Construction B3

In this test, we conduct to approximate a Riemann solution of Construction B3 with the Riemann data:

$$U_0(x) = \begin{cases} U_L = (h_L, u_L, \theta_L, a_L) = (0.5, 2, 4, 1.5) \in G_2, & \text{if } x < 0, \\ U_R = (h_R, u_R, \theta_R, a_R) = (0.9, 1.5, 3, 1) \in G_2, & \text{if } x > 0. \end{cases} \tag{5.11}$$

Table 20 Errors of numerical approximations and orders of accuracy for different mesh sizes for test 6 in the interval of rarefaction wave $(-0.0875, -0.0461)$

	Godunov-type scheme		Superbee limiter		van Leer's limiter	
N	$\|\|U_h - U\|\|_{L^1}$	Order	$\|\|U_h - U\|\|_{L^1}$	Order	$\|\|U_h - U\|\|_{L^1}$	Order
1600	0.0013		4.5596×10^{-4}		4.5645×10^{-4}	
3200	7.9636×10^{-4}	0.65	2.3483×10^{-4}	0.95	2.3479×10^{-4}	0.96
6400	4.9920×10^{-4}	0.67	1.2497×10^{-4}	0.91	1.2494×10^{-4}	0.91

Table 21 Errors of numerical approximations and orders of accuracy for different mesh sizes for test 6 in the interval of rarefaction wave (0.4059, 0.4420)

	Godunov-type scheme		Superbee limiter		van Leer's limiter	
N	$\|\|U_h - U\|\|_{L^1}$	Order	$\|\|U_h - U\|\|_{L^1}$	Order	$\|\|U_h - U\|\|_{L^1}$	Order
1600	0.0015		2.9277×10^{-4}		2.9749×10^{-4}	
3200	0.0011	0.50	1.5151×10^{-4}	0.95	1.5465×10^{-4}	0.94
6400	7.2782×10^{-4}	0.57	7.8238×10^{-5}	0.95	8.0580×10^{-5}	0.94

According to Construction B3, the exact solution is started by a 1-rarefaction wave from U_L to U_1, then followed by a stationary wave from U_1 to U_2, then followed by a 1-shock wave with zero speed from U_2 to U_3, then followed by a stationary wave U_3 to U_4, then followed by a 2-contact wave from U_4 to U_5, then followed by a 3-shock wave from U_5 to U_R, where $U_L, U_1, U_2, U_3, U_4, U_5, U_R$ are reported in Table 22.

As seen in (3.6), the exact solution contains three waves propagating with the same zero speed.

Figure 32 shows an exact solution and its approximation at time $t = 0.05$ on the interval $[-1, 1]$ with 100 mesh points by the van Leer-type scheme using the superbee limiter or van Leer's limiter, and by the Godunov-type scheme. The errors of solution and orders of accuracy for test 7 are reported in Table 23 and the errors of solutions are also showed in Fig. 33.

Again, the errors for approximating solutions of both schemes tend to zero as the mesh sizes tend to zero, as shown in Table 23 and Fig. 33, and the errors of van Leer-type scheme are much smaller than the ones of Godunov-type scheme. In addition,

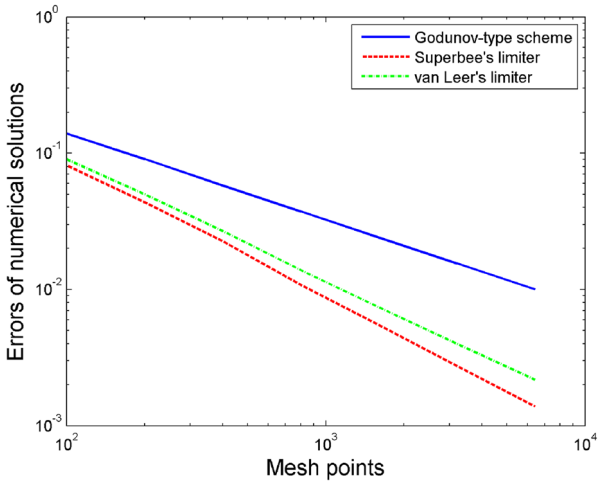

Fig. 29 Errors of numerical solutions with different mesh points for test 6

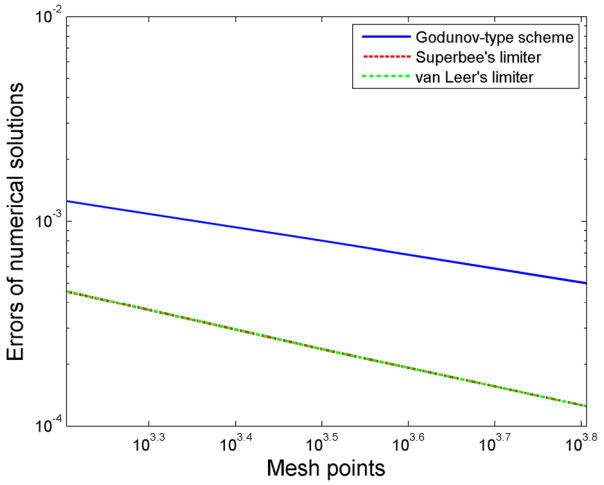

Fig. 30 Errors of numerical solutions with different mesh points in the interval of rarefaction wave $(-0.0875, -0.0461)$ for test 6

the orders of accuracy of van Leer-type scheme are higher than the ones of Godunov-type scheme; and we also see these outcomes as in Table 24 and Fig. 34 when we consider the interval $(-0.1114, 0.0000)$ containing rarefaction wave.

Consequently, test 7 demonstrates the convergence of the approximate solutions by the van Leer-type scheme to the exact solution in this very interesting *resonant case*, where the exact solution contains several waves corresponding to different characteristic fields, which propagate with a coinciding shock speed. Especially, the van Leer-type scheme using the superbee limiter has a better accuracy than the one using the van Leer limiter.

5.8 Test 8: Interaction of waves

In this test, we consider the Cauchy problem where the initial data consist of three constant states U_L, U_M, and U_R with two different jump discontinuities at $x_1 = 0$ and $x_2 = 1$. First of all, the Cauchy problem can be seen as two separated Riemann problems located at x_1 and x_2. After a certain time $t = t_1$, the highest speed wave in the solution of the Riemann problem located at x_1 interacts with the lowest speed

Table 22 States that separate the elementary waves of the exact solution of the Riemann problem in test 7: Construction B3

	U_L	U_1	U_2	U_3	U_4	U_5	U_R
h	0.5	0.333950	0.168242	0.586556	0.785290	0.906775	0.9
u	2.0	3.618124	7.181757	2.059946	1.538632	1.538632	1.5
θ	4.0	4.0	4.0	4.0	4.0	3.0	3.0
a	1.5	1.5	1.174806	1.174806	1.0	1.0	1.0

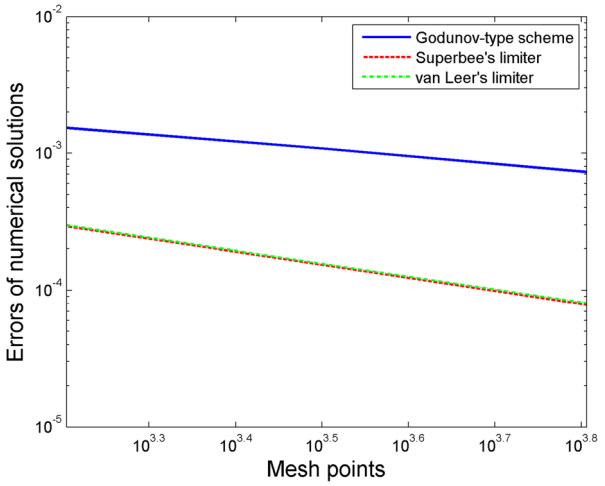

Fig. 31 Errors of numerical solutions with different mesh points in the interval of rarefaction wave (0.4059, 0.4420) for test 6

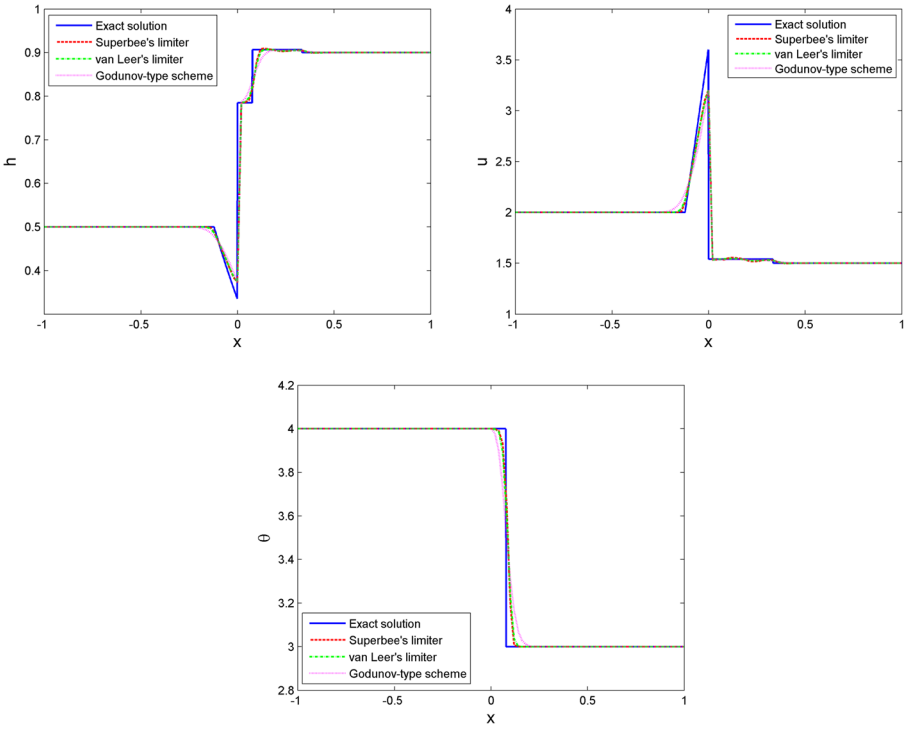

Fig. 32 Exact and approximate solutions with 100 mesh points for test 7

Table 23 Errors of numerical approximations and orders of accuracy for different mesh sizes for test 7

	Godunov-type scheme		Superbee limiter		van Leer's limiter	
N	$\|\|U_h - U\|\|_{L^1}$	Order	$\|\|U_h - U\|\|_{L^1}$	Order	$\|\|U_h - U\|\|_{L^1}$	Order
100	0.1033		0.0735		0.0770	
200	0.0670	0.62	0.0396	0.89	0.0430	0.84
400	0.0425	0.66	0.0203	0.96	0.0233	0.89
800	0.0269	0.66	0.0114	0.83	0.0132	0.82
1600	0.0171	0.66	0.0053	1.10	0.0068	0.95
3200	0.0109	0.64	0.0026	1.02	0.0037	0.90
6400	0.0070	0.63	0.0013	0.97	0.0020	0.86

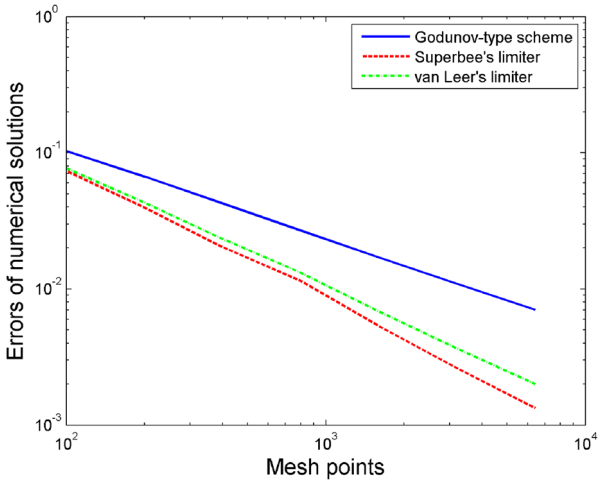

Fig. 33 Errors of numerical solutions with different mesh points for test 7

Table 24 Errors of numerical approximations and orders of accuracy for different mesh sizes for test 7 in the interval of rarefaction wave $(-0.1114, 0.0000)$

	Godunov-type scheme		Superbee limiter		van Leer's limiter	
N	$\|\|U_h - U\|\|_{L^1}$	Order	$\|\|U_h - U\|\|_{L^1}$	Order	$\|\|U_h - U\|\|_{L^1}$	Order
100	0.0145		0.0085		0.0090	
200	0.0093	0.63	0.0045	0.93	0.0047	0.95
400	0.0078	0.25	0.0033	0.45	0.0034	0.44
800	0.0054	0.53	0.0020	0.74	0.0021	0.74
1600	0.0035	0.63	0.0011	0.83	0.0012	0.83
3200	0.0021	0.77	5.6169×10^{-4}	0.98	5.8911×10^{-4}	0.98
6400	0.0012	0.79	2.8658×10^{-4}	0.97	3.0092×10^{-4}	0.97

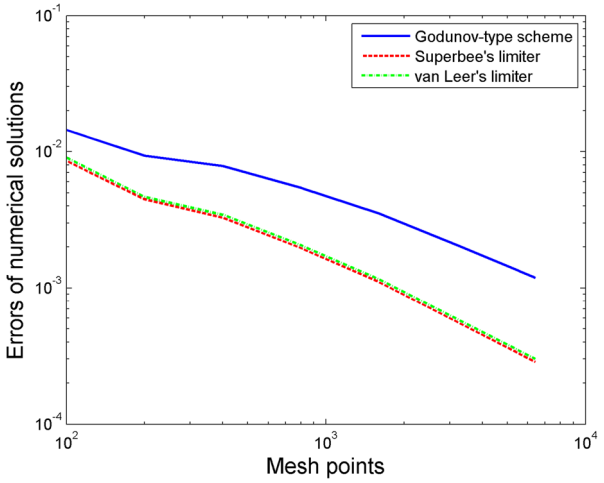

Fig. 34 Errors of numerical solutions with different mesh points in the interval of rarefaction wave for Test 7

wave in the solution of the Riemann problem located at x_2 generating new waves after the wave interaction at t_1. We will point out the time of wave interaction t_1; simultaneously, we will approximate solution by the our scheme after this time and compare with the exact solution. It is interesting to see the interaction of waves where the bottom level suffers a jump. Therefore, we will consider the interaction of a 3-shock starting from x_1 with a 4-stationary contact discontinuity along x_2. This two waves meet at $(x, t) = (x_2, t_1)$. New waves are generated from this interaction of wave, and they are merely elementary waves of the local Riemann problem located at (x_2, t_1).

Specifically, we consider the Cauchy problem with the following initial condition

$$U_0(x) = \begin{cases} U_L = (h_L, u_L, \theta_L, a_L) = (0.5, 6, 3, 1.2) \in G_1, & \text{if } x < 0, \\ U_M = (h_M, u_M, \theta_M, a_M) = (0.3, 5, 4, 1) \in G_1, & \text{if } 0 < x < 1, \\ U_R = (h_R, u_R, \theta_R, a_R) = (0.199774, 7.508502, 4, 0.7) \in G_1, & \text{if } x > 1, \end{cases} \tag{5.12}$$

see Fig. 35.

Obviously, the Riemann data (U_L, U_M) at $x = 0$ satisfies construction A1 and the Riemann data (U_M, U_R) at $x = 1$ satisfies (2.26). So, while $t < t_1$, the Riemann solution at $x = 0$ is

$$W_4(U_L, U_1) \oplus S_1(U_1, U_2) \oplus W_2(U_2, U_3) \oplus S_3(U_3, U_M),$$

and the Riemann solution at $x = 1$ is just the 4-contact stationary wave

$$W_4(U_M, U_R),$$

(see Fig. 36). An interaction of wave occurs when the 3-shock wave $S_3(U_3, U_M)$ from $x = 0$ meets the 4-stationary contact wave $W_4(U_M, U_R)$ at $(x = 1, t_1)$. The

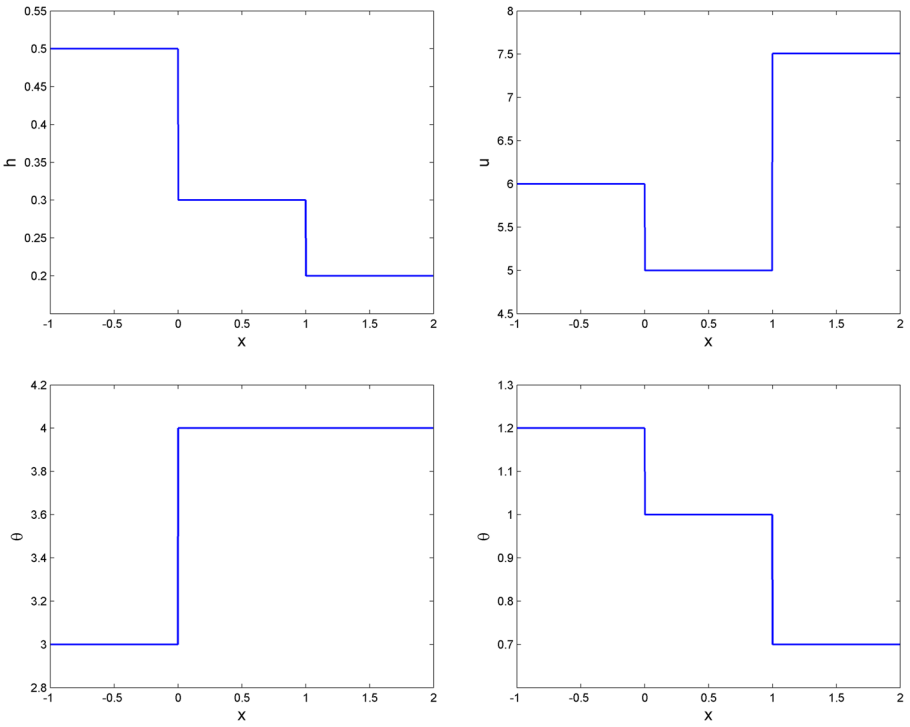

Fig. 35 The initial condition (5.12)

time t_1 is determined by equating

$$x = \sigma_3(U_3, U_R)t = 1,$$

or

$$t_1 \approx 0.1039.$$

Observe that the 2-contact $W_2(U_2, U_3)$ starting at $x = 0$ may meet the 4-contact $W_4(U_M, U_R)$ at a larger time t_2, when the line $x = \sigma_2(U_2, U_3)t$ cuts the line $x = 1$. It is easy to check that

$$t_2 \approx 0.1541.$$

We will conduct the test at a time t_* between these two values t_1 and t_2. For instance, we take

$$t_* = 0.15.$$

Note that after the first interaction of wave between the 3-shock wave $S_3(U_3, U_M)$ and the 4-stationary contact wave $W_4(U_M, U_R)$, new waves are generated and form a solution of the local Riemann problem located at $(x = 1, t_1)$ with the initial data (U_3, U_R). It is easy to see that after the first wave interaction and before the second interaction of wave, that is

$$t_1 < t < t_2,$$

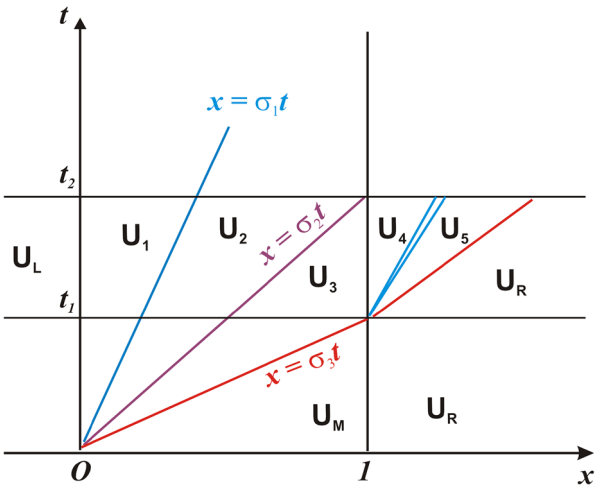

Fig. 36 The exact solution for test 8 at time $t_1 < t < t_2$

the exact solution of this local Riemann problem located at $(x = 1, t_1)$ with the initial data (U_3, U_R) is given by

$$W_4(U_3, U_4) \oplus R_1(U_4, U_5) \oplus S_3(U_5, U_R).$$

Thus, the exact solution for (1.1) with initial data (5.12) at the time $t = 0.15$ is

$$W_4(U_L, U_1) \oplus S_1(U_1, U_2) \oplus W_2(U_2, U_3) \oplus W_4(U_3, U_4) \oplus R_1(U_4, U_5) \oplus S_3(U_5, U_R),$$

(see Fig. 36) where U_1, U_2, U_3, U_4, and U_5 are reported in Table 25.

Figure 37 shows an exact solution and its approximation at time $t = 0.15$ on the interval $[-1, 2]$ with 100 mesh points by the van Leer-type scheme using the superbee limiter or van Leer's limiter and the Godunov-type scheme. Besides that, the errors of solution and orders of accuracy for this test are reported in Table 26 and the errors of solutions are also showed in Fig. 38.

Apparently, the approximate solutions of both schemes tend to the exact solution when the mesh sizes tend to zero, as shown in Table 26 and Fig. 38. The errors of van Leer-type scheme are much smaller than the ones of Godunov-type scheme. In addition, the orders of accuracy of van Leer-type scheme are higher than the ones of Godunov-type scheme; and we also have the likely results as in Table 27 and

Table 25 States that separate the elementary waves of the exact solution of the Riemann problem in test 8: Interaction of waves

	U_1	U_2	U_3	U_4	U_5
h	0.412437	0.510408	0.442026	0.333005	0.308126
u	7.273842	6.487368	6.487368	8.611240	8.886406
θ	3.0	3.0	4.0	4.0	4.0
a	1.0	1.0	1.0	0.7	0.7

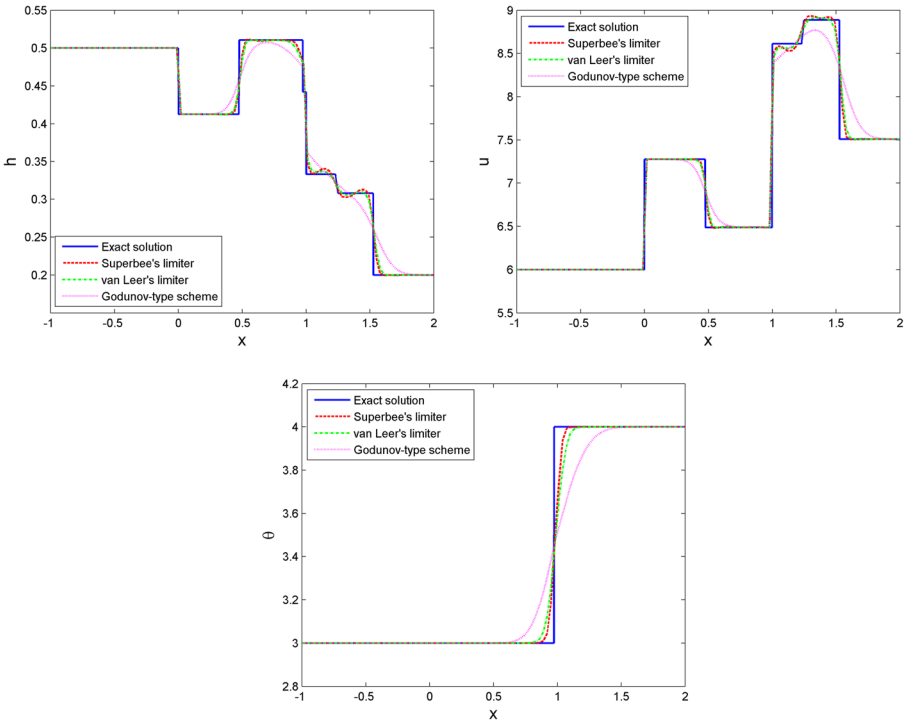

Fig. 37 Exact and approximate solutions with 100 mesh points for test 8

Fig. 39 when we consider the interval (1.2207, 1.2597) containing rarefaction wave, the tendency of the orders of accuracy gradually increase in case the mesh points get bigger. Furthermore, our van Leer-type scheme using the superbee limiter has a better accuracy than the one using the van Leer limiter as in Table 26.

Thus, this test also demonstrates the convergence of the approximate solutions by the van Leer-type scheme to the exact solution.

Table 26 Errors of numerical approximations and orders of accuracy for different mesh sizes for test 8

	Godunov-type scheme		Superbee limiter		van Leer's limiter	
N	$\|\|U_h - U\|\|_{L^1}$	Order	$\|\|U_h - U\|\|_{L^1}$	Order	$\|\|U_h - U\|\|_{L^1}$	Order
100	0.3761		0.0974		0.1309	
200	0.2368	0.67	0.0473	1.04	0.0629	1.06
400	0.1543	0.62	0.0329	0.52	0.0405	0.63
800	0.0924	0.74	0.0133	1.31	0.0184	1.14
1600	0.0573	0.69	0.0078	0.76	0.0108	0.77
3200	0.0352	0.70	0.0043	0.86	0.0060	0.86
6400	0.0223	0.66	0.0025	0.77	0.0034	0.81

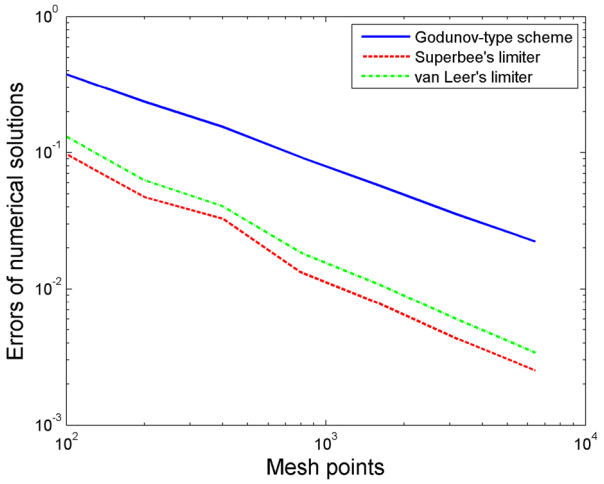

Fig. 38 Errors of numerical solutions with different mesh points for test 8

Table 27 Errors of numerical approximations and orders of accuracy for different mesh sizes for test 8 in the interval of rarefaction wave (1.2207, 1.2597)

	Godunov-type scheme		Superbee limiter		van Leer's limiter	
N	$\|\|U_h - U\|\|_{L^1}$	Order	$\|\|U_h - U\|\|_{L^1}$	Order	$\|\|U_h - U\|\|_{L^1}$	Order
1600	0.0024		5.9773×10^{-4}		3.7429×10^{-4}	
3200	0.0020	0.26	4.2734×10^{-4}	0.48	1.9418×10^{-4}	0.95
6400	0.0016	0.34	2.2644×10^{-4}	0.92	9.9061×10^{-5}	0.97

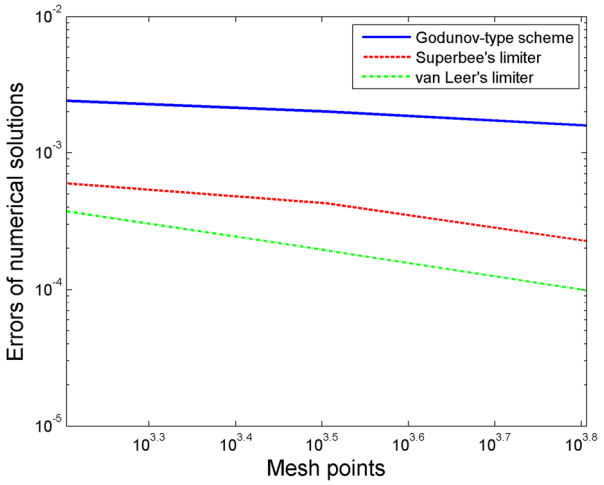

Fig. 39 Errors of numerical solutions with different mesh points in the interval of rarefaction wave for test 8

6 Conclusions

Our second-order van Leer-type scheme constructed in this work for the Ripa system (1.1) is shown by tests to be quite in the well-balanced sense as it can exactly capture the stationary smooth solutions as well as stationary elementary discontinuities. It can work well for data in the supercritical region or subcritical region, or both. All the tests show that the approximate solutions by the scheme converge to the exact solutions. Besides that, the tests demonstrate that the errors and orders of accuracy of van Leer-type scheme are better than the ones of Godunov-type scheme. Furthermore, the approximate solutions of van Leer-type scheme using the superbee limiter have a better accuracy than ones that use van Leer's limiter. However, in some cases, the van Leer-type scheme using the superbee limiter may suffer a slight oscillation, which will almost disappear for small enough mesh sizes.

Acknowledgments The author would like to thank the reviewers for their very constructive comments and fruitful discussions. This research is funded by Vietnam National Foundation for Science and Technology Development (NAFOSTED) under grant number **"101.02-2019.306"**.

Funding This research is funded by Vietnam National Foundation for Science and Technology Development (NAFOSTED) under grant number "101.02-2019.306."

References

1. Ambroso, A., Chalons, C., Coquel, F., Galié, T.: Relaxation and numerical approximation of a two-fluid two-pressure diphasic model. Math. Mod. Numer. Anal. **43**, 1063–1097 (2009)
2. Ambroso, A., Chalons, C., Raviart, P.-A.: A Godunov-type method for the seven-equation model of compressible two-phase flow. Computers & Fluids **54**, 67–91 (2012)
3. Audusse, E., Bouchut, F., Bristeau, M.-O., Klein, R., Perthame, B.: A fast and stable well-balanced scheme with hydrostatic reconstruction for shallow water flows. SIAM J. Sci Comput. **25**, 2050–2065 (2004)
4. Baudin, M., Coquel, F., Tran, Q.-H.: A semi-implicit relaxation scheme for modeling two-phase flow in a pipeline. SIAM J. Sci. Comput. **27**, 914–936 (2005)
5. Botchorishvili, R., Perthame, B., Vasseur, A.: Equilibrium schemes for scalar conservation laws with stiff sources. Math. Comput. **72**, 131–157 (2003)
6. Botchorishvili, R., Pironneau, O.: Finite volume schemes with equilibrium type discretization of source terms for scalar conservation laws. J. Comput. Phys. **187**, 391–427 (2003)
7. Chinnayya, A., LeRoux, A.-Y., Seguin, N.: A well-balanced numerical scheme for the approximation of the shallow water equations with topography: the resonance phenomenon. Int. J. Finite Vol. **1**(4), 33 (2004)
8. Chertock, A., Kurganov, A., Liu, Y.: Central-upwind schemes for the system of shallow water equations with horizontal temperature gradients. Num. Math. **127**, 595–639 (2014)
9. Cuong, D.H., Thanh, M.D.: A well-balanced van Leer-type numerical scheme for shallow water equations with variable topography. Adv. Comput. Math. **43**, 1197–1225 (2017)
10. Cuong, D.H., Thanh, M.D.: A high-resolution van Leer-type scheme for a model of fluid flows in a nozzle with variable cross-section. J. Korean Math. Soc. **54**(1), 141–175 (2017)
11. Coquel, F., Hérard, J.-M., Saleh, K., Seguin, N.: Two properties of two-velocity two-pressure models for two-phase flows. Commun. Math. Sci. **12**, 593–600 (2014)
12. Dal Maso, G., LeFloch, P.G., Murat, F.: Definition and weak stability of nonconservative products. J. Math. Pures Appl. **74**, 483–548 (1995)
13. Desveaux, V., Zenk, M., Berthon, C., Klingenberg, C.: Well-balanced schemes to capture non-explicit steady states: Ripa model. Math. Comp. **85**, 1571–1602 (2016)

14. Gallardo, J.M., Parés, C., Castro, M.: On a well-balanced high-order finite volume scheme for shallow water equations with topography and dry areas. J. Comput. Phys. **227**, 574–601 (2007)
15. Gallouet, T., Herard, J.-M., Seguin, N.: Some approximate Godunov schemes to compute shallow-water equations with topography. Comput. & Fluids **32**, 479–513 (2003)
16. Godlewski, E., Raviart, P.-A.: Numerical approximation of hyperbolic systems of conservation laws springer (1996)
17. Greenberg, J.M., Leroux, A.Y.: A well-balanced scheme for the numerical processing of source terms in hyperbolic equations. SIAM J. Numer. Anal. **33**, 1–16 (1996)
18. Han, X., Li, G.: Well-balanced finite difference WENO schemes for the Ripa model. Comput. Fluids **134-135**, 1–10 (2016)
19. Hou, T.Y., LeFloch, P.: Why nonconservative schemes converge to wrong solutions. Error analysis Math. of Comput. **62**, 497–530 (1994)
20. Kröner, D., Thanh, M.D.: Numerical solutions to compressible flows in a nozzle with variable cross-section. SIAM J. Numer. Anal. **43**, 796–824 (2005)
21. LeFloch, P.G., Thanh, M.D.: A Godunov-type method for the shallow water equations with variable topography in the resonant regime. J. Comput. Phys. **230**, 7631–7660 (2011)
22. Li, G., Caleffi, V., Qi, Z.K.: A well-balanced finite difference WENO scheme for shallow water flow model. Appl. Math. Comput. **265**, 1–16 (2015)
23. Li, G., Song, L.N., Gao, J.M.: High order well-balanced discontinuous Galerkin methods based on hydrostatic reconstruction for shallow water equations. J. Comput. Appl. Math. **340**, 546–560 (2018)
24. Qian, S.G., Shao, F.J., Li, G.: High order well-balanced discontinuous Galerkin methods for shallow water flow under temperature fields. Comput. Appl. Math. **37**, 5775–5794 (2018)
25. collab= P. Ripa: Conservation laws for primitive equations models with inhomogeneous layers. Geophys Astrophys Fluid Dyn. **70**, 85–111 (1993)
26. Ripa, P.: On improving a one-layer ocean model with thermodynamics. J. Fluid Mech. **303**, 169–201 (1995)
27. Rosatti, G., Begnudelli, L.: The Riemann Problem for the one-dimensional, free-surface shallow water equations with a bed step: theoretical analysis and numerical simulations. J. Comput. Phys. **229**, 760–787 (2010)
28. Sanchez-Linares, C., Morales de Luna, T., Castro Diaz, M.J.: A HLLC scheme for Ripa model. Appl. Math. Comput. **72**, 369–384 (2016)
29. Saurel, R., Abgrall, R.: A multi-phase Godunov method for compressible multifluid and multiphase flows. J. Comput. Phys. **150**, 425–467 (1999)
30. Tian, B., Toro, E.F., Castro, C.E.: A path-conservative method for a five-equation model of two-phase flow with an HLLC-type Riemann solver. Comput. & Fluids **46**, 122–132 (2011)
31. Thanh, M.D.: The Riemann problem for the shallow water equations with horizontal temperature gradients. Appl. Math. Comput. **325**, 159–178 (2018)
32. Thanh, M.D., Thanh, N.X.: Well-balanced numerical schemes for shallow water equations with horizontal temperature gradient. Bull. Malays. Math. Sci. Soc **43**(1), 783–807 (2020). https://doi.org/10.1007/s40840-018-00713-5
33. Thanh, N.X., Thanh, M.D., Cuong, D.H.: Godunov-type numerical scheme for the shallow water equations with horizontal temperature gradient. Taiwan. J. Math. **24**(1), 179–223 (2020). https://doi.org/10.11650/tjm/190501
34. Touma, R., Klingenberg, C.: Well-balanced central finite volume methods for the Ripa system. Appl. Num. Math. **97**, 42–68 (2015)